Molecular Therapy
Nucleic Acids
Original Article

Selection of DNA aptamers that prevent the fibrillization of α-synuclein protein in cellular and mouse models

Erin M. McConnell,[1] Dennis Chan,[3] Katelyn Ventura,[3] Joshua P. Callahan,[1] Kathryn Harris,[3] Vernon H. Hunt,[1] Spencer Boisjoli,[1] Daniel Knight,[1] Evan T. Monk,[1] Matthew R. Holahan,[3] and Maria C. DeRosa[1,2]

[1]Department of Chemistry, Carleton University, Ottawa, ON K1S 5B6, Canada; [2]Institute of Biochemistry, Carleton University, Ottawa, ON K1S 5B6, Canada; [3]Department of Neuroscience, Carleton University, Ottawa, ON K1S 5B6, Canada

A neuropathological hallmark of Parkinson's disease (PD) is the aggregation and spreading of misfolded α-synuclein (αSyn) protein. In this study, a selection method was developed to identify aptamers that showed affinity for monomeric αSyn and inhibition of αSyn aggregation. Aptamer a-syn-1 exhibited strong inhibition of αSyn aggregation *in vitro* by transmission electron microscopy and Thioflavin T fluorescence. A-syn-1-treated SH-SY5Y cells incubated with pre-formed fibrils (PFFs) showed less intracellular aggregation of αSyn in comparison with a scrambled oligonucleotide control, as observed with fluorescent microscopy. Systemic delivery of a-syn-1 to the brain was achieved using a liposome vehicle and confirmed with fluorescence microscopy and qPCR. Transgenic mice overexpressing the human A53T variant of αSyn protein were injected with a-syn-1 loaded liposomes at 5 months of age both acutely (single intraperitoneal [i.p.] injection) and repeatedly (5 i.p. injections over 5 days). Western blot protein quantification revealed that both acute and repeated injections of a-syn-1 decreased levels of the aggregated form of αSyn in the transgenic mice in the prefrontal cortex, caudate, and substania nigra (SNc). These results provide *in vitro* and *in vivo* evidence that a-syn-1 can inhibit pathological αSyn aggregation and may have implications in treatment strategies to target dysregulation in PD.

INTRODUCTION

Parkinson's disease (PD) affects 2%–3% of the global population over the age of 65, making it the second most common progressive neurodegenerative disorder worldwide.[1] Cardinal symptoms comprise resting tremor, postural instability, rigidity, bradykinesia, and stooped posture.[2] The emergence of these motor symptoms is linked with the progressive loss of dopaminergic neurons located within the substantia nigra (SNc).[3] While the clinical diagnosis of PD relies on the development of motor symptoms, prodromal non-motor symptoms emerge oftentimes in advance of the motor symptoms suggestive of a disease progression that starts well before clinical diagnosis.[4]

A common pathological feature underlying the etiology of PD is the misfolding and fibrilization of the α-synuclein protein (αSyn).[5] αSyn is a polypeptide 140 amino acids in length and encoded by the SNCA gene.[6] The protein is principally observed in native monomeric forms at the presynaptic terminal in the brain as well as in other tissues, namely the gastrointestinal tract and the heart.[4] Under normal physiological conditions, αSyn is typically found as either soluble monomer or tetramer. A hallmark of PD pathology occurs once soluble αSyn monomers aggregate into insoluble oligomers and protofibrils.[7] Aggregation begins with soluble αSyn monomers being phosphorylated, which can promote oligomer species and insoluble fibril formation.[8,9] Folded αSyn monomers turn into unfolded monomers that aggregate into dimers, oligomers, and then into amyloid conformations.[5] This sets off a disease process that leads to neuron death and progression from neuron to neuron. The non-amyloid β component (NAC) region of αSyn is believed to be the origin of misfolding and aggregation,[10] specifically between amino acids 71 and 81.[5,11]

Although PD pathology is closely associated with αSyn aggregation, numerous PD models fail to capture the development of αSyn aggregates.[12–14] The αSyn pre-formed fibril (PFF) model can trigger the aggregation of αSyn and induce neuronal loss.[15] In this model, αSyn PFFs are generated from agitating αSyn monomers. These generated αSyn PFFs can then be used to trigger endogenous αSyn monomers to misfold in model systems.[16]

As a complement to the PFF model, a commercially available transgenic mouse, originally made by Lee and colleagues, has been instrumental in linking αSyn oligomerization with the PD-like phenotype.[17] These mice express the human A53T variant αSyn and, at approximately 8 to 14 months of age, develop an increasingly severe motor phenotype including impaired movement, partial limb paralysis, tremor, and incapacity to stand.[17] Immunohistochemistry

Received 26 March 2023; accepted 13 June 2024;
https://doi.org/10.1016/j.omtn.2024.102251.

Correspondence: Matthew R. Holahan, Department of Neuroscience, Carleton University, Ottawa, ON K1S 5B6, Canada.
E-mail: matthew.holahan@carleton.ca
Correspondence: Maria C. DeRosa, Department of Chemistry, Carleton University, Ottawa, ON K1S 5B6, Canada.
E-mail: maria.derosa@carleton.ca

data from these mice as early as 3 months of age reveals αSyn aggregation in the motor cortex and thalamus.[18] αSyn aggregate inclusions appear prior to observation of motor impairment.[18] The inclusions in neurons are composed primarily of αSyn fibrils (10–16 nm in length), as confirmed by immunoelectron microscopy and biochemical analysis.[17] What is observed in these mice, in terms of the timing, location, and structure of these inclusions, mimics what is seen in human neuronal α-synucleinopathies, including familial PD.

The primary purpose of this work was to select αSyn binding aptamers that inhibit or prevent protein aggregation. Aptamers are functional nucleic acids that are derived via an iterative selection process called systematic evolution of ligands by exponential enrichment (SELEX).[19,20] Briefly, a single-stranded DNA or RNA library containing 10^{13} to 10^{15} molecules is incubated with the target molecule. Sequences with affinity to the target are partitioned from those with negligible affinity for the target. An enriched library is then created by amplifying those binding sequences, and this is the input for the next round of selection. Typically, selections are 5–15 rounds long and yield aptamers with affinity (K_d) in the nanomolar to low micromolar range.[21] Aptamers form distinct 3-dimensional secondary structures that enable their interaction with high affinity and selectivity to a cognate target. Targets of successful aptamer selections range from small molecules to whole cells.[21] Though functionally similar to antibodies and other synthetic receptors, aptamers have several advantages over these other molecular recognition tools.[22] Aptamers are synthetically produced, can be easily chemically modified, exhibit good bioavailability and biocompatibility, and have a long shelf-life.[22,23] Further, the intrinsic chemical properties of nucleic acids provide an inherent antidote to any aptamer-based therapeutic in the aptamer sequence complement.[24]

There exists unique potential for the application of aptamers in neurodegenerative diseases. Currently, no effective molecular therapies exist for protein abnormality implicated neurodegenerative diseases, particularly PD. A unifying strategy is to select aptamers that can decrease the production of pathogenic protein, inhibit the formation of pathogenic aggregates, or degrade pathogenic aggregates. Additionally, the potential of aptamers for neurodegenerative diseases offers innovative delivery methods to bypass the blood-brain barrier (BBB). These methods involve encapsulating aptamers into modified liposomes[25] or exosomes[26] to enhance the efficiency of aptamer delivery to targeted brain regions. For example, two DNA aptamers, F5R1 and F5R2, were packaged within modified RVG-exosomes, demonstrating the capability of aptamers to traverse the BBB, bind to PFFs, and inhibit αSyn aggregation in the brain.[26] Other aptamers have been selected for their capacity to specifically bind amyloid-beta peptide and mutant huntingtin protein to prevent aggregation.[27,28] Aptamers for PrP^{Sc} have also been shown to inhibit prion propagation.[29] Details of progress toward these efforts has been recently reviewed elsewhere.[28] The potential of aptamers for diagnosing, studying, and treating PD has been demonstrated by a handful of aptamer selection and/or characterization studies. Five selections have reported aptamers with affinity to monomer, oligomer, or fibril αSyn.[30–34] The aptamers described in these studies have reported K_Ds in the low to mid nanomolar range, and almost all of the papers reported at least one aptamer with demonstrated inhibitory effect on αSyn aggregation. A detailed summary of these studies is provided in Table S1. Additionally, their potential therapeutic applications were previously described.[35] Generally, the selection strategies entailed a search for aptamers that bound to αSyn, followed by an assessment of αSyn binding and the inhibitory activity of those hits following selection. However, the consensus in the aptamer literature is that, in order to ensure optimal fit for purpose, aptamer selection experiments should be designed with the eventual application in mind and that conditions of the selection should match as best as possible to those of the application.[36] Thus, if the eventual goal of the aptamer is to inhibit aggregation, it was important to intentionally employ conditions that would encourage αSyn aggregation during the selection experiment and then set up an appropriate partitioning step such that sequences that survived the selection were inhibitory in nature. Ultimately, this strategy is described here and was successful; in particular, one aptamer, **a-syn-1** was found to prevent fibrillization in *in vitro* assays and in a cellular PFF model. **A-syn-1** binding was confirmed *in vitro* by DNase assay and impedance spectroscopy and also *in vivo* by fluorescence co-localization. **A-syn-1** was also shown to reduce oligomer αSyn when it was packaged into a targeting liposome vehicle and delivered systemically in the transgenic A53T mouse model system. Results from this work provide a fundamental strategy for development of therapeutic tools for the study and treatment of PD.

RESULTS

Selection of αSyn binding DNA aptamers

In this work, a new method for the selection of aptamers that prevent the fibrillization of αSyn was developed. Two templates comprised the DNA library used for this selection experiment. One template contained a 30-base random region. The other template was based on an existing αSyn binding aptamer (M5-15) shown to have some affinity for the monomer form.[31] The central domain of the M5-15 aptamer-based template was mutated from the parent aptamer sequence by 30%, whereas the novel template contained a completely randomized region. The selection strategy employed is represented schematically in Figure 1.

In this method, the selection of aptamers began with the incubation of the DNA library in a 1:1 ratio with αSyn (Figure 1: step 1). An extended incubation period compared with typical selection experiments was employed to encourage protein aggregation and to create a stringent selection pressure toward aptamers that bound to and retained the monomer state of αSyn (Figure 1: step 2). Following the incubation period, ultracentrifugation (Figure 1: step 3) was used to separate the following fractions: unbound aptamer, aptamer bound to monomer, aptamer bound to small oligomers (dimers, trimers, or tetramers), and aptamer bound to large oligomers (fibrils and large aggregates). Next, the fractions were exposed to an extended

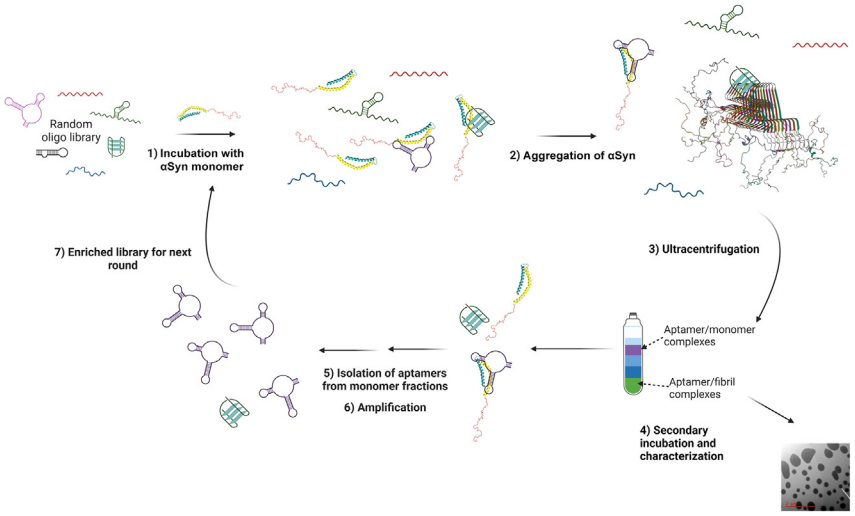

Figure 1. Schematic representation of SELEX experiment for the discovery of aptamer-based inhibitors of αSyn aggregation

First, a naive DNA oligonucleotide library was incubated with the monomer αSyn (1). Aggregation was induced (2) and specific monomer protein-binding aptamers were isolated by ultracentrifugation (3). The fractions that contained aptamers with inhibitory potential were identified by transmission electron microscopy and fluorescence spectroscopy (4). Those selected fractions were subjected to a nitrocellulose filtration (5) to remove unbound DNA, then the binding DNA was recovered by phenol-chloroform extraction. Following amplification (6) of the extracted DNA, the enriched DNA library (7) was subjected to another round of selection.

secondary incubation step. This step was critical as it allowed fractions of interest (those that showed monomer binding as well as inhibition) to be distinguished from fractions that showed monomer binding alone (Figure 1: step 4). The fractions expected to contain aptamers with inhibitory properties (those that remained in aptamer-monomer complex over extended incubation time) were then subjected to nitrocellulose filtration (Figure 1: step 5). Following the nitrocellulose filtration, protein-bound aptamer that had been retained on the filter was isolated by phenol-chloroform extraction. The DNA hits could then be amplified by polymerase chain reaction (Figure 1: step 6) resulting in an enriched DNA pool (Figure 1: step 7) ready for the beginning of another selection round.

During the optimization and selection process, polyacrylamide gel electrophoresis (PAGE) was employed to resolve which fractions held αSyn monomer, tetramer, or aggregate, using a protein ladder control for comparison. From the expected mass of these αSyn forms and the estimated size of the DNA library, it could be determined in which fraction the αSyn monomer-DNA complex could be expected to be found, as well as the fractions containing unbound monomer and free DNA, and the fractions containing different sized αSyn aggregates bound to DNA. These fractions were further characterized using transmission electron microscopy (TEM) (Figure S1). These images displayed a marked difference in the protein conformations observed in each fraction. It appeared that the DNA library was able to somewhat abate aggregation of αSyn protein, as can be noted by comparing the dimensions and morphology of features imaged in fractions 4, 14, and 20 (Figure S1) to the control images where αSyn aggregation proceeded in the absence of the library. On balance, the presence of the DNA yielded much smaller protein structures.

Since the selection library contained the M5-15 aptamer and its mutants, it was necessary to judge the inhibitory effect of the previously published M5-15 aptamer. The ability of the M5-15 aptamer to prevent fibrillization was examined in the preparation of fibrils, following the MJFF protocol. Fibril formation, which was comparable to the control (no DNA) reaction, was noted despite the presence of the M5-15 aptamer (Figure S2).

High-throughput sequencing and structural analysis of aptamer candidates

Following five rounds of selection, aptamer candidates were identified by high-throughput sequencing (HTS) using Illumina MiSeq sequencing technology. HTS technology provided sequencing information that was then analyzed using the AptaSuite software developed by the Przytycka research group.[37] Using AptaSuite, five aptamer candidates were identified from millions of sequences by comparing the enrichment value and pool fraction (individual sequence count/total number of sequences). RNAStructure modeling (on the DNA setting) predicted the secondary structures of the aptamers.[38] See Figure S3 for structures of the aptamer candidates alongside the predicted secondary structure of M5-15. A detailed analysis of the sequencing data for each aptamer candidate is provided in the supplemental material (Table S2). Multiple stem loop motifs, not unlike what is observed in the M5-15 aptamer, were predicted for the hits, varying in complexity from two-way to four-way junctions.[39] Interestingly, most of the aptamer candidates were enriched in A content, decreased in G content, and had similar C and T content compared with the M5-15 aptamer (Figure S4).

Inhibitory effect of the aptamer candidates on αSyn aggregation *in vitro*

The ability of the aptamer hits to hinder formation of fibrils was investigated. PFFs from αSyn monomer were generated as described for the control reaction.[40,41] Thioflavin T fluorescence enhancement assay was employed to compare the effect of the aptamer sequences on protein aggregation. At day 7, the control solution of αSyn alone showed a material increase in fluorescence, confirming protein aggregation. By contrast, samples containing αSyn and aptamer showed little to no ThT fluorescence, suggesting that the aptamers had an inhibitory effect (Figure S5). Electron microscopy was also used to

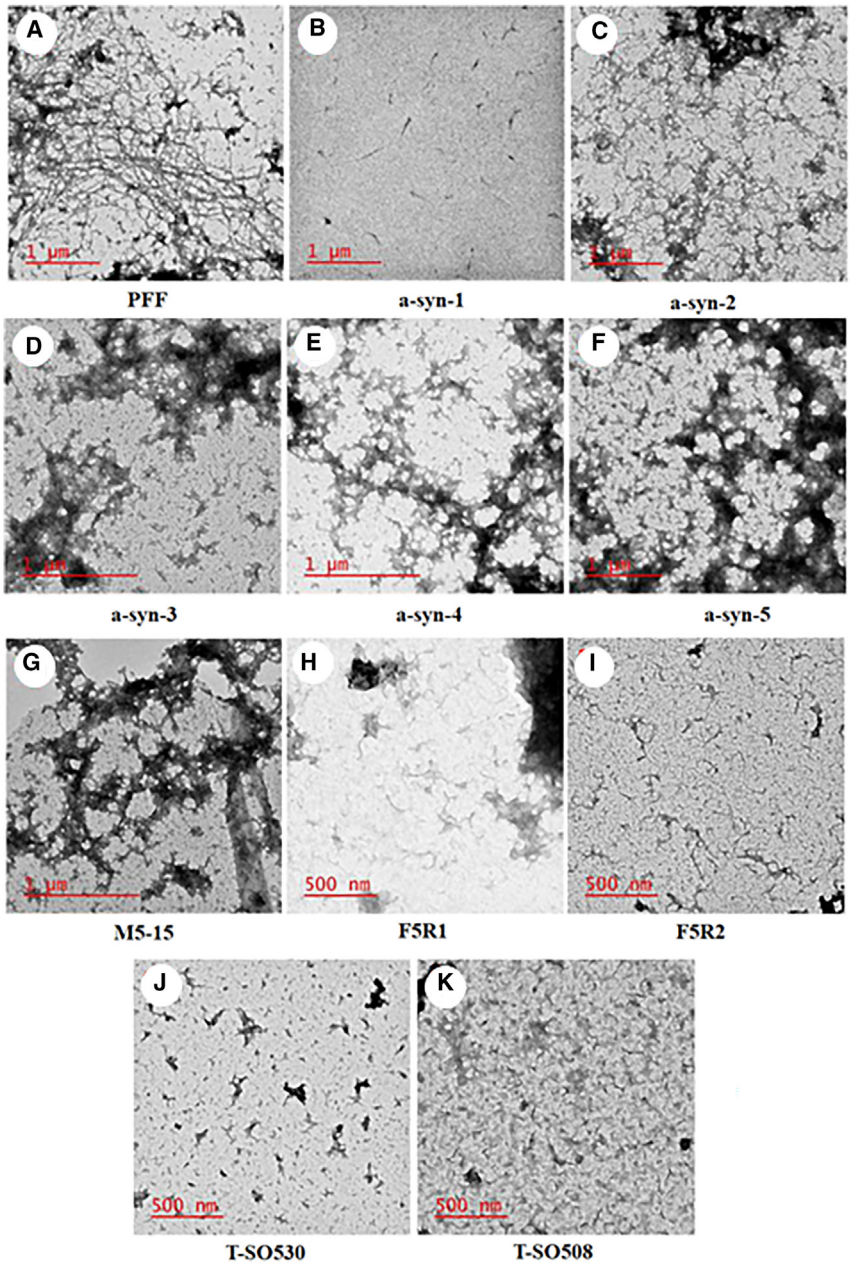

Figure 2. Electron microscopy is a standard method for determining protein aggregation state

Transmission electron microscopy (TEM) imaging was used to examine the inhibitory effect on αSyn pre-formed fibrils (PFFs) (A) of the aptamer candidates (B–F), the M5-15 control (G), and other αSyn binding aptamers (H–K), and on fibril formation after a 7-day incubation period. Representative images are shown. Aptamers were incubated for 7 days in the presence of an αSyn PFF at 37°C with constant agitation. All images were obtained in aptamer:protein molar ratios of 10:1. Scale bars shown are either 1 μm or 500 nm.

investigate protein morphology following a 7-day incubation period. Images of the control reaction compared with images containing the aptamer candidates (Figure S6) revealed clear differences in protein morphology. In the absence of an aptamer candidate, fibrils could be seen (Control: Figure S6). Incubation with **a-syn-1** aptamer led to the presence of much smaller, spherical to amorphous morphology. The inhibitory effect of the remaining aptamer candidates was less pronounced. In each case, though extensive fibrillization was not observed, the formation of larger micron-sized, morphology was present (Figure S6). Similar conditions were repeated to assess the effect on protein inhibition of the aptamers, other published aptamers,[31–33] and the M5-15 control sequence[30]; imaging was performed using TEM. Comparable trends were observed, where **a-syn-1** showed the most dramatic effect on fibril inhibition. Representative images are shown in Figure 2.

In vitro evaluation of a-syn-1 aptamer-αSyn monomer binding affinity

Given that the most promising hit from the initial inhibition assay was **a-syn-1**, the binding affinity of that aptamer to monomer protein was characterized *in vitro* by two assays, a footprinting assay using DNase I[42] and an electrochemical impedance spectroscopy assay (EIS). In the footprinting assay, the 5′-fluorescently labeled aptamer and monomer αSyn were incubated first together for a brief period then with DNase I. It was expected that the aptamer would be digested by the DNase I differently depending on the interaction of the DNA with target. After a brief incubation period, the digestion reaction was quenched by the addition of the metal ion chelator, EDTA, then analyzed by PAGE. The DNA footprint was visualized by the excitation of the 5′-fluorescent dye. The DNA footprint of **a-syn-1** and monomer αSyn is shown in Figure S7. The αSyn monomer concentration-dependent differences in relative band intensity were used to fit the apparent dissociation constant (K_D) of the complex. The M5-15 aptamer, which has been shown to have affinity for αSyn monomer, was used as a positive control (Figure S8). The apparent K_D of the **a-syn-1** aptamer-monomer αSyn complex was 28 ± 14 nM. The apparent K_D of the M5-15 aptamer-monomer αSyn complex was determined to be 142 ± 39 nM.

Since the K_D value of an aptamer for its target can depend strongly on the method used to assess this interaction, it is important to assess K_D using multiple techniques.[36,43] The data described above represent binding free in solution, which is most appropriate for the inhibition application. In the EIS assay, the **a-syn-1** aptamer was immobilized on a gold electrode surface and electrochemical changes in charge

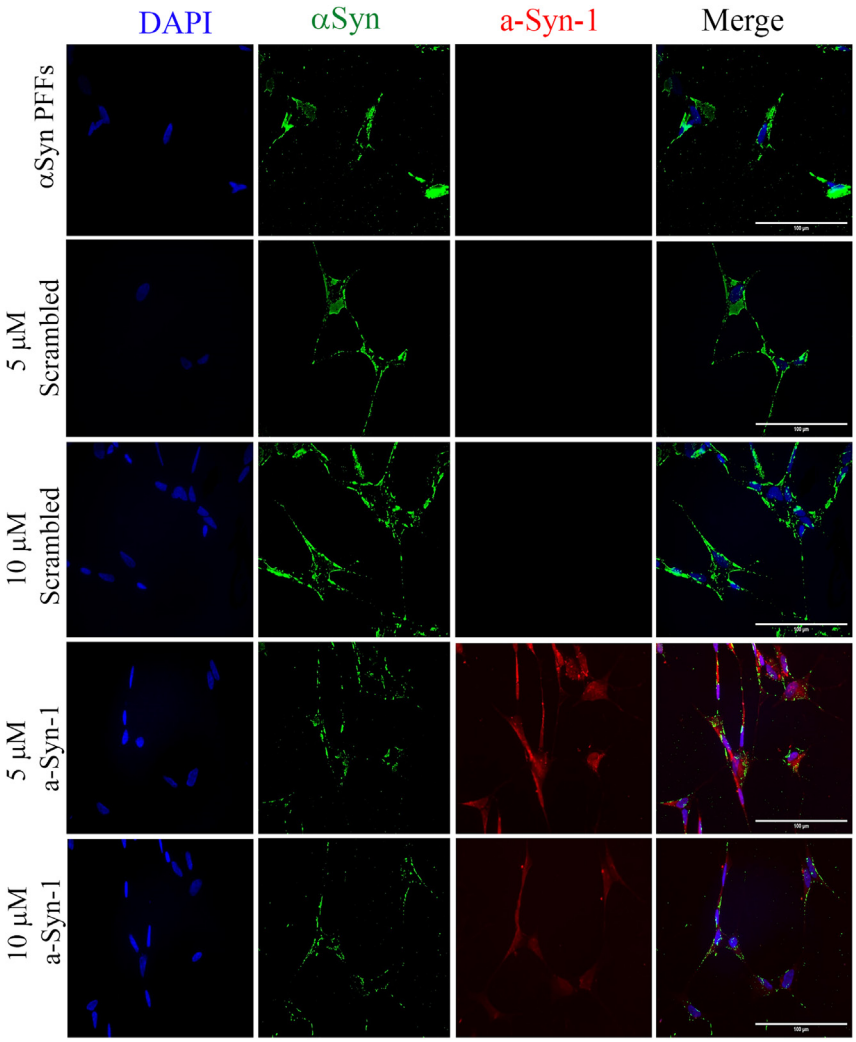

Figure 3. Determination of a-syn-1 inhibitory activity in a cellular model

DNA aptamer, **a-syn-1**, impedes αSyn aggregation induced by αSyn PFFs in differentiated SH-SY5Y cells. Immunofluorescence staining of αSyn aggregation following incubation of αSyn PFFs at 8 h. Scale bar, 100 μm. Blue = DAPI; Green = anti-αSyn filament antibody/Alexa Fluro Plus 488 secondary antibody; Red = CY5-labeled **a-syn-1**.

transfer resistance (R_{ct}) were monitored in the presence of monomeric αSyn (see Figures S9 and S10). The calculated K_D of the **a-syn-1** aptamer-monomer αSyn complex was 70 ± 3 nM using this technique.

The EIS assay also confirmed the selectivity of **a-syn-1** (see Figure S11). Binding of **a-syn-1** to synuclein proteins (α-, β-, γ-synuclein), αSyn fibrillar form, monomeric A53T-mutant αSyn, $A\beta_{1-40}$, and thrombin were evaluated. The concentrations of monomeric αSyn and A53T-mutant were 1 μM while other control targets were all 10 μM. **A-syn-1** displayed specificity toward both A53T-mutant and monomeric αSyn when compared with fibrillar αSyn and other target proteins. Indeed, the aptamer displayed, 3-fold tighter binding toward the A53T-mutant, suggesting an alanine to threonine point mutation significantly enhances complex formation while immobilized. The selectivity of the **a-syn-1** aptamer for multiple synuclein (α, A53T wild type, beta, and gamma) was qualitatively assessed by microscale thermophoresis (MST: Figure S12).[44] This technique, which relies on target-dependent changes in the thermophoretic properties (size, charge, hydration shell) of an aptamer versus an aptamer bound to its target, has proven useful for binding analyses. Within the range of concentrations assessed by this method, **a-syn-1** and protein binding was observed to be similar between αSyn monomer and A53T mutant αSyn. In contrast, no binding was observed for the **a-syn-1** aptamer to either β-synuclein or γ-synuclein.

Impact of a-syn-1 on αSyn aggregation in SH-SY5Y cells

Subsequently, the capacity of the DNA aptamer, **a-syn-1**, to impede αSyn aggregation was tested in a cellular model, where pre-formed αSyn fibrils (PFFs) are incubated with SH-SY5Y cells to promote αSyn accumulation and aggregation (Figures 3 and 4). Optimization of the cellular model is described in the supplemental information (Figures S13 and S14). For this experiment either αSyn PFFs alone or combined with **a-syn-1**, were incubated with the cells, and the temporal pattern of αSyn aggregation (1, 2, 4, and 8 h) was monitored. To justify that the DNA aptamer sequence of **a-syn-1** was unique and prevented αSyn aggregate accumulation, it was compared with a scrambled DNA sequence of similar length and composition to a separate set of differentiated SH-SY5Y cells.

The change in αSyn aggregation was analyzed using a two-way fixed factor ANOVA, with treatment and time as the factors. The results of the two-way ANOVA indicated that no statistically significant interaction between treatment and time existed in relation to αSyn aggregation ($F_{(12,\ 40)} = 1.12$, $p > 0.05$), whereas the main effects of treatment ($F_{(3,\ 40)} = 45.08$, $p < 0.001$) and time ($F_{(3,\ 40)} = 35.66$, $p > 0.05$) were significantly different. Post hoc analyses demonstrated no significant difference in αSyn aggregation between scrambled oligonucleotide control and αSyn PFFs alone ($p > 0.05$). In contrast, SH-SY5Y cells that were co-incubated with 5 μM or 10 μM **a-syn-1**, exhibited a significant decrease in αSyn aggregation compared with αSyn PFFs alone ($p < 0.001$). Notably, treatment with 5 μM **a-syn-1** reduced αSyn aggregation by 46%, whereas 10 μM **a-syn-1** resulted

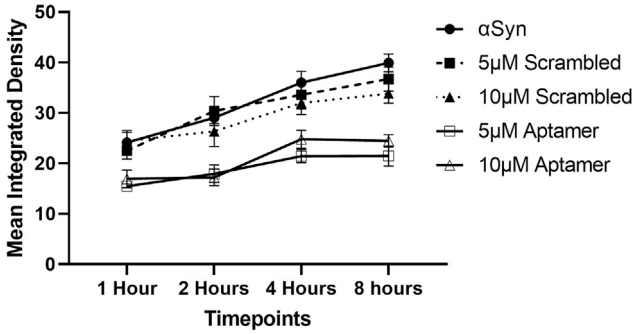

Figure 4. Comparison of effects of the DNA aptamer, a-syn-1, and control scrambled DNA sequences on αSyn aggregation in differentiated SH-SY5Y cells

All values represent average mean integrated density against αSyn PFF treatment group. Error bars represent SEM. Significant differences between 5 μM or 10 μM aptamer compared with αSyn PFFs alone was noted by Tukey's HSD post hoc analysis, $p < 0.001$.

in a 38% maximum reduction. These results suggest that the specific sequence of the DNA aptamer, **a-syn-1**, can reduce αSyn aggregation in a cellular PFF model.

In vivo delivery and action of a-syn-1

In order to assess the inhibitory potential of **a-syn-1** in a transgenic mouse model, a vehicle for delivery of the aptamer across the BBB was required. The liposome delivery system that was employed, known as transferrin receptor aptamer modified (TRAM) liposomes, has been characterized previously.[25] Briefly, a-syn-TRAM is a targeting liposome loaded with the **a-syn-1** aptamer and also modified with a second aptamer that recognizes the transferrin receptor, which is highly expressed on the BBB. TRAM liposomes are surface PEGylated and tagged with the transferrin receptor aptamer via a thioether conjugation between a thiol-modified aptamer and a maleimide-modified lipid.

a-syn-TRAM Liposomes (0.1 mL) were injected intraperitoneally (i.p.) into either B6C3F1/J mice or transgenic (A53T) mice. Each dose was estimated to have 1.5×10^{13} liposomes and 15 ± 6 aptamers per liposome.[45] This equated to a dosage of approximately 0.22 ± 0.09 mg/kg of aptamer delivered via the 1X liposome suspension, and a loading efficiency of 10% ± 4% to 12% ± 4% based on a typical reaction volume of 1,000–1,200 μL (see Tables S6–S8 for calculations). Mice were euthanized 30 min after a-syn-TRAM i.p. injections and brains of the transgenic mice were extracted to assess the presence of the **a-syn-1** aptamer in brain tissue by fluorescence microscopy, while qPCR was used to assess biodistribution in liver and brain at 15 min, 30 min, 1 h, and 2 h post injection in the wild-type mice. The Cq value is the polymerase chain reaction (PCR) cycle number at which the sample's reaction curve intersects the threshold line and is inversely proportional to the amount of target nucleic acid in the sample. Thus, a reduction in Cq in comparison with an empty vehicle control is indicative of the presence of the aptamer sequence. Figure 5A shows the average Cq values from motor cortex homogenate (the tabulated values can be found in Table S9). A significant **a-syn-1** volume × time interaction ($F_{(6,68)} = 4.82$, $p < 0.001$) was revealed by ANOVA. Tukey's honestly significant difference (HSD) tests revealed that at 15 min, both aptamer doses were associated with reduced Mean Cq value, while at 30 min, only 200 μL of **a-syn-1** was associated with reduced Cq values ($p < 0.001$). No significant differences were detected 1 or 2 h after **a-syn-1** administration. Figure 5B shows the average Cq values for midbrain homogenates (the tabulated values can be found in Table S10). A significant interaction between **a-syn-1** volume and time ($F_{(11,68)} = 7.69$, $p < 0.001$) was revealed by ANOVA. Follow-up tests confirmed that the 100 μL and 200 μL **a-syn-1** were associated with reduced Cq values throughout ($p < 0.001$) except for a less pronounced effect of 200 μL 1 h following treatment ($p = 0.077$). The average Cq values from liver homogenate can be found in Figure 5C (the tabulated values can be found in Table S11). A significant main effect of the **a-syn-1** aptamer volume ($F_{(2,17)} = 41.490$, $p < 0.001$) and a significant interaction between volume and time ($F_{(11,68)} = 4.562$, $p < 0.001$) were revealed by ANOVA. Tukey's HSD tests of the aptamer main effect revealed the Cq values for both volumes were reduced compared to the empty liposome control condition at all four time points. Follow-up Tukey's HSD tests on the interaction revealed that this reduction was less pronounced at 1 h compared with the other time points. Thus, aptamer can be detected after injections of either doses within both the motor cortex and the midbrain after only 15 min. Aptamer persists for 30 min within the motor cortex and can be detected within the midbrain even after 2 h from the higher dose. In contrast, the aptamer can be strongly detected in the liver from either dose through to the 2-h time point, as would be expected given the expression of transferrin receptor in the liver.

Fluorescence microscopy was used to assess aptamer localization with αSyn target *in vivo*. Selective phosphorylation of Ser129 is known to be widespread in synucleinopathy lesions and to encourage insoluble fibril formation.[46] Fluorescence microscopy was used to determine the localization of the secondary antibody fluorescence (green) from the phospho-specific anti-αSyn antibody and the fluorescence from the Cy3.5-labeled **a-syn-1** aptamer (red) (Figure 6) as well as their proximity to each other. The confocal images show that the phospho-specific αSyn antibody (green) is closely apposed to the **a-syn-1** aptamer (red) potentially within a neuron (inset of Figure 6), consistent with delivery of the aptamer and interaction with the αSyn target.

Changes in αSyn aggregation with aptamer administration investigated by western blot

Western blot analysis using the anti-αSyn, oligomer-specific Syn33 antibody of different brain regions allowed for assessment of **a-syn-1** administration on αSyn aggregation.[47] Gel images are shown in Figure S15. This antibody targets aggregated αSyn and has been confirmed with multiple assays.[47] To assess the impact of **a-syn-1** on αSyn levels *in vivo*, the aptamer was once again packaged in a TRAM-liposome vehicle capable of transport across the BBB[25] and injected into mice expressing the human A53T variant of αSyn.

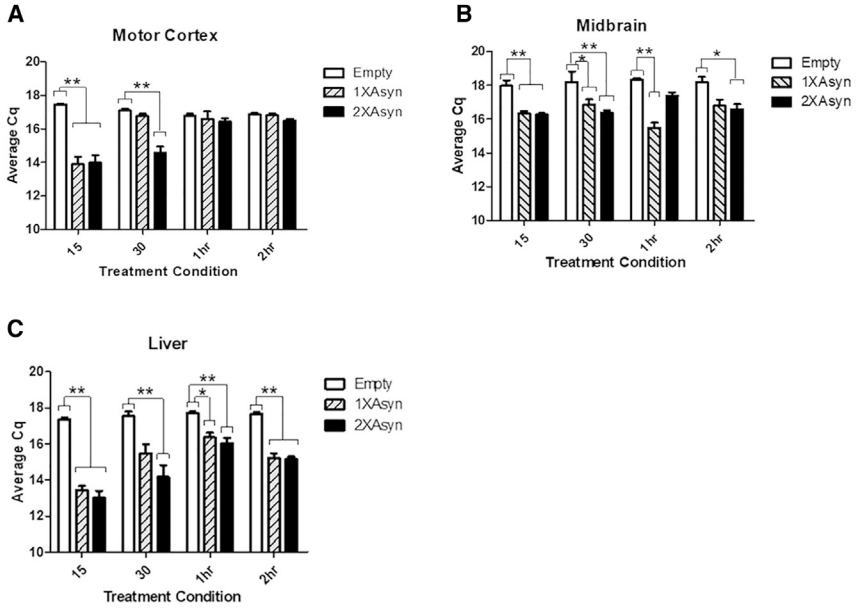

Figure 5. Real-time quantitative PCR was used to assess a-syn-1 presence in brain tissue

Average quantification cycle (Cq) detected for **a-syn-1** in (A) motor cortex, (B) midbrain, and (C) liver for B6C3F1/J male mice treated with 100 μL **a-syn-1** (1X Asyn), 200 μL **a-syn-1** (2X Asyn), or control treatment (empty liposome). All values represent average Cq values ± SEM. Significant differences determined by Tukey's HSD post hoc analysis denoted by $*p < 0.05$; $**p < 0.01$.

Mice in the control group received 100 μL injections of 0.9% saline daily for 5 days. The single treatment group received 100 μL of TRAM loaded with **a-syn-1** on the first day followed by daily saline injections for the remaining 4 days. Mice in the multiple treatment group received daily injections of TRAM loaded with **a-syn-1** or a scrambled oligonucleotide control for the 5 consecutive days. All mice were rapidly decapitated 7 days following the last injection. The experimental timeline is summarized in Figure 7.

Three, separate one-way ANOVAs were conducted for the normalized Syn33 (oligomeric form) levels within the prefrontal cortex (Figure 7A), the caudate putamen (Figure 7B), and the substantia nigra (Figure 7C). These analyses revealed a main effect of treatment within all three brain regions (PFC: $F_{(4,25)} = 5.344$, $p < 0.01$; Caudate: $F_{(4,25)} = 10.403$, $p < 0.01$; SNc: $F_{(4,25)} = 3.914$ $p < 0.014$). In the PFC, the multi **a-syn-1** treatment group showed lower Syn33 levels than all other groups ($*p < 0.05$). In the caudate, Syn33 levels were significantly higher in the Tg control and scrambled treatment groups compared with all other groups ($*p < 0.05$) indicating that single and multi **a-syn-1** treatments reduced oligomeric αSyn levels to control values. In the SNc, the scrambled sequence group showed higher levels of Syn33 than the wild-type (WT) control treatment and the single and multi **a-syn-1** treatment groups ($***p < 0.01$). Taken together, these data confirm a significant and specific inhibitory effect of the aptamer on αSyn aggregation after systemic administration.

DISCUSSION

PD is a progressive, incurable condition whose observable symptoms may not be revealed until several years after onset. While l-DOPA therapy is initially able to alleviate PD symptoms, its effectiveness wanes over time causing motor complications to return within approximately 5 years.[48,49] As a result, alternative strategies have been pursued to mitigate symptoms over a longer duration. Unfortunately, a consistent pattern has emerged of the return of motor symptoms following multiple years of drug therapy.[48,50–53]

The design of the SELEX experiment encouraged the selection of αSyn aggregation inhibitors

In the present study, DNA aptamers that bind to αSyn in the monomer or small oligomer state were selected and characterized *in vitro*.[54] Demonstrated precedence motivated the use of a selection pool derived from a mutated aptamer sequence, which successfully produced high-affinity aptamers.[21,55] To date, five aptamers have been reported with demonstrated inhibitory activity both *in vitro* (typically by microscopy) and in models, as well as human tissue; their selection and characterization details are summarized in Table S1. Compared with the αSyn aptamers that have been described recently, the selection method herein is the only one that intentionally selected for inhibitory aptamers by judiciously designing selection conditions that favored strong aggregation inhibitors. For example, two selection templates were combined to create one selection library. It has been previously demonstrated that using a pool derived from a mutated aptamer sequence can successfully produce high-affinity aptamers[55] and that the use of multiple pools has been shown to improve selection outcome.[21] Beyond that, inclusion of the M5-15 aptamer and its mutants added stringency to the selection. M5-15 was confirmed to bind strongly to αSyn but not inhibit its aggregation. By mixing the mutant library with the randomized one, the top sequence candidates had to outcompete αSyn binders and prevent inhibition in order to survive the selection.

With each round, conditions of the selection experiment were also varied to increase the stringency of the selection pressure to yield better inhibitors (e.g., by increasing the incubation period and encouraging aggregation) rather than to find better binders (e.g., by decreasing the target concentration).[37,38] The incubation period of the final selection round was 13 days. This long incubation period was used to increase the stringency of the selection, so that only aptamers that had strong inhibitory ability, target affinity, and stability would survive the selection. Furthermore, incorporating the ultracentrifugation step as a method to separate aptamer-protein complexes allowed for the selective partitioning of the monomer-binding

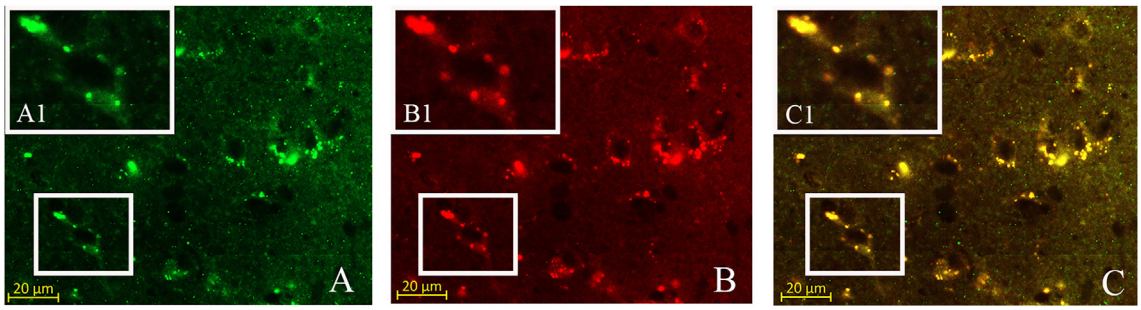

Figure 6. The distribution of a-syn-1 aptamer in midbrain tissue was assessed after an acute injection of a-syn-TRAM liposome by fluorescence microscopy
(A) Green: anti-αSyn (phospho S129) antibody. (B) Red: fluorescently (Cy3.5) labeled aptamer. (C) Yellow: Image overlay showing fluorescence apposition. (A1), (B1), and (C1) insets are magnified versions of the feature highlighted by the white boxes in each panel. Scale bar denotes 20 μm.

fraction of the library. The results suggest that this approach was successful and that this extended incubation-ultracentrifugation SELEX could be universally adapted to multiple protein targets of interest where mass-based separation of different protein forms is desired.

Visualization of protein morphology by electron microscopy was essential in monitoring the successful progression of the selection experiment. The purpose of the ultracentrifugation step was to separate the aptamer bound to different protein conformations by mass prior to imaging, therefore the results observed in Figure S1 may seem counterintuitive. Fraction 4 (Figure S1) was expected to contain free DNA and free monomer, and therefore it would be reasonable to observe similar sized protein in the control and library-treated samples. The differences in size of the protein observed between the free DNA/free monomer control and library fractions can be explained by the secondary incubation that occurred post ultracentrifugation. This secondary incubation was key to observing the inhibitory effect of the selection library by electron microscopy imaging. In the absence of DNA library, some of the monomer protein aggregated, explaining the difference in size observed in the TEM images obtained from fraction 4 for each condition. A similar argument can be used to explain the size differences observed for fraction 14. Fraction 14 was expected to contain aptamer bound to monomer as well as smaller αSyn oligomers (dimer, trimer, tetramer).[5,56] During the secondary incubation, the DNA bound to monomer and smaller oligomers had an inhibitory effect, protecting the protein from further aggregation. In the absence of DNA, the protein aggregated further resulting in a drastic difference in the size of the observed aggregates in the control fraction 14. A similar, yet less drastic effect is observed between fraction 20. This is likely because in this case, the DNA was bound to larger aggregates from the outset of the secondary incubation.

A-syn-1 can selectively bind αSyn and abate its aggregation *in vitro*

The propensity of the newly selected aptamer hits to lessen αSyn aggregation was investigated *in vitro* using standard techniques for monitoring protein morphology and aggregation state. In this first experiment, the inhibitory capacity of each aptamer on the formation of fibrils was assessed by scanning electron microscopy (SEM) (Figure S6). A marked difference was observed in the morphology of the protein incubated with **a-syn-1** aptamer and αSyn compared with the DNA free protein control. This assay was repeated, and reactions were imaged using TEM, which allowed for more detailed imaging (Figure 2). Again, **a-syn-1** inhibited aggregate and fibril formation and the effect was more dramatic than what was observed for other αSyn aptamers from this selection or from the literature. Finally, the ability of the selected aptamer hits to inhibit αSyn aggregation was assessed by the Thioflavin T assay, by which aggregation inhibition in the presence of aptamer was observed (Figure S5). Considered together, these data suggest that the **a-syn-1** aptamer is the most promising aggregation inhibitor among the group of aptamer hits and compares favorably with other αSyn aptamers from the literature. Thus, **a-syn-1** served as the primary aptamer candidate for study in a cellular model.

While the goal of this selection was not to find the best αSyn binder, it was still important to confirm binding affinity and specificity of our top aptamer hit. Our work confirmed that **a-syn-1,** either while free in solution or tethered to a surface, binds with good affinity and specificity to αSyn monomer. Notably, the affinity of **a-syn-1** was also assessed in an organic electrolyte gated field effect transistor aptasensor system, where the aptamer was immobilized on a surface during sensing. The K_D determined in this work was 6.6 pM, several orders of magnitude less (higher affinity) than the best K_D of the previously reported aptamers for αSyn.[54] There are multiple factors that will influence whether or not the K_D of an aptamer changes when it is immobilized.[57] It is likely in this case that the secondary structure was stabilized by immobilization, leading to the improved affinity.

A-syn-1 can reduce the aggregation of αSyn in SH-SY5Y cells and in the A53T transgenic mouse model

In this study, the αSyn PFF model was used in differentiated SH-SY5Y cells. Results showed that without the DNA aptamer, αSyn aggregation was predominately found near the nucleus. SH-SY5Y cells treated with **a-syn-1** showed a significant decrease in αSyn aggregation and displayed a diffuse distribution of αSyn in the cellular body and neurite projections. These changes were not noted in cells treated with the scrambled oligonucleotide control (Figures 3 and

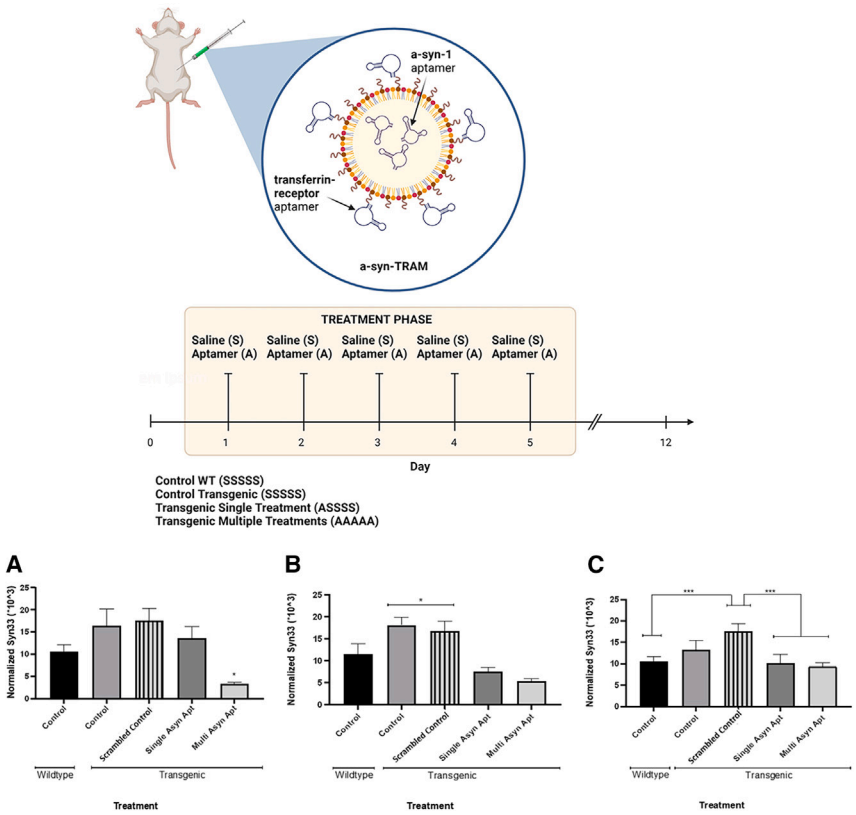

Figure 7. Reduction in αSyn oligomer levels following systemic injections of a-syn-1 in A53T mice

Top: Experimental timeline representation for the *in vivo* assessment of **a-syn-1.** Wild-type (WT) or transgenic (A53T) mice began the treatment regimen at 5 months of age (D0). Mice were treated with saline (S) or aptamer/scrambled (A) on the days indicated. As an example, the Control WT mice were treated with saline (S) for the 5 treatment days (SSSSS); the Transgenic Multiple Treatment group was treated with **a-syn-1** aptamer or scrambled loaded in the targeting a-syn-TRAM liposome(A) for the 5 days (AAAAA). All mice were euthanized (EOS) 7 days after the last treatment (D12). Bottom: Normalized Syn33 protein levels ($\times 10^3$) in the (A) prefrontal cortex (PFC), (B) caudate, and (C) substantia nigra (SNc). WT and Tg B6; C3-Tg(Prnp-SNCA*A53T)83Vle/J male mice treated with saline or **a-syn-1** aptamer (acutely (single) or repeatedly (multi)). Values represent average ± SEM. In the PFC, the multi **a-syn-1** treatment group showed less Syn33 levels than all other groups ($^*p < 0.05$). In the caudate, Syn33 levels were significantly higher in the Tg control and scrambled treatment groups compared with all other groups ($^*p < 0.05$) indicating that single and multi **a-syn-1** treatments reduced Syn33 levels to control values. In the SNc, the scrambled sequence group showed higher levels of Syn33 then the WT control treatment and the single and multi **a-syn-1** treatment groups ($^{***}p < 0.01$). Figure created in Biorender.

4). These findings demonstrate the ability of **a-syn-1** to penetrate the cell membrane, saturate the cell, and localize in close apposition to the nucleus. Interestingly, no difference was found between the reduction of αSyn aggregation caused by 5 μM or 10 μM **a-syn-1** ($p > 0.05$); future work will examine a full dose-response dependence.

With evidence to support the inhibitory properties of **a-syn-1**, the *in vivo* experiments were next attempted to assess the effectiveness of the aptamer to reduce aggregation of transgenic αSyn protein, requiring a vehicle for delivery of the aptamer across the BBB in an animal model. A key observation from this set of experiments is that the TRAM liposome approach can deliver **a-syn-1** across the BBB. The aptamer was found in different areas in the brain (and in the liver) by qPCR. As predicted given the intraperitoneal administration, the liver had the highest levels of the **a-syn-1** aptamer immediately following treatment. Remarkably, within just 15 min of administration, the motor cortex and midbrain regions were also found to contain aptamer (Figure 5). Fluorescence staining and imaging of *ex vivo* tissue slices also revealed binding of the **a-syn-1** aptamer to αSyn protein in the brain (Figure 6). Apposition of the phospho S129 anti-αSyn antibody with Cy3.5 labeled **a-syn-1** aptamer confirmed that the aptamer could be delivered across the BBB via the targeting liposomes and that once there, the **a-syn-1** aptamer can interact with αSyn *in vivo*. These findings, as well as those in previous work,[25] highlight similar delivery capabilities with other delivery methods such as modified exosomes.[26]

The A53T transgenic (Tg) mouse model was then utilized to assess the ability of systemically administered **a-syn-1** to reduce aggregation of αSyn in brain tissue (Figure 7). The A53T Tg mice injected with saline showed increased levels of Syn33 staining compared with WT controls treated with saline. This is to be expected, as mice expressing the A53T human αSyn exhibit increased neuronal αSyn aggregates.[58] A single systemic treatment with the **a-syn-1** aptamer had a moderate effect in reducing Syn33 levels in the substantia nigra, a more pronounced effect in the caudate. In the repeated **a-syn-1** treatment group, there was a more consistent reduction in Syn33 levels across the three brain regions investigated. The caudate and prefrontal cortex both showed significant reductions compared with the control Tg mice. In the SNc, the effect was present but not to the same extent as the other brain regions. These data demonstrate that once-a-day injections of the **a-syn-1** aptamer over 5 days are effective in reducing αSyn aggregation *in vivo*. The specificity of the **a-syn-1** sequence is shown when compared with the scrambled sequence that had no effect in reducing levels of Syn33.

Through *in vivo* experiments, it was demonstrated that an aptamer selected to bind to αSyn and impair its aggregation could reduce features of PD in a mouse model without obvious immediate unfavorable effects. After multiple injections, **a-syn-1** (but not the scrambled oligonucleotide control) reduced levels of oligomer αSyn (Syn33; aggregated form of αSyn) in the caudate, substantia nigra, and cortex. Overall, this work offers a fundamental strategy for promising

therapeutic tools by targeting αSyn monomers to halt αSyn pathology. It is still unclear, however, if this approach can abate both motor and non-motor symptoms, influence the progression of the disorder, and develop tolerance from repeated use.

Beyond the potential therapeutic uses of the αSyn aptamer described herein, it could also serve as the recognition element of an "aptasensor" for diagnostic purposes. In fact, **a-syn-1** was recently adapted to detect αSyn in spiked human saliva using a prototype microdevice for non-invasive point-of-care testing with a demonstrated linear detection range of 100 fg/L to 10 μg/L.[54] A diagnostic device that can identify elevated levels of αSyn prior to the onset of other symptoms could revolutionize early diagnosis and consequently disease intervention.

Conclusion

A key component contributing to the neurodegenerative processes underlying PD includes the aggregation of αSyn. Misfolded αSyn protein dimers become oligomers to form insoluble fibrils leading to aggregation that can trigger cell death and other toxic signals. The abnormal aggregation of αSyn appears to play a critical role in the cellular damage associated with PD. In this report, an aptamer was selected and characterized for its ability to reduce αSyn aggregation and fibrillization. This DNA aptamer, **a-syn-1**, also bound intracellularly to monomeric αSyn protein and prevented aggregation in SH-SY5Y cells. These results provide *in vitro* evidence that the **a-syn-1** aptamer can inhibit the pathological response of αSyn aggregation in neurons. Further, this work suggests it is possible for an αSyn aptamer to gain access to the brain via systemic administration, using a transferrin receptor targeting liposome as a vehicle, and that repeated treatments with the aptamer can yield a reduction in oligomer αSyn concentrations. With a more complete understanding of how the aptamer derails the pathological processes underlying PD, the next step is to test the *in vivo* capacity at stopping, slowing, or even reversing αSyn aggregation and fibrillization. An aptamer "supplement" capable of impeding the toxic consequences of αSyn accumulation could have major implications on both the study and treatment of PD.

MATERIALS AND METHODS

Preparation of oligonucleotides

A MerMade 6 DNA synthesizer (BioAutomation, Irving, TX, USA) was used to prepare the oligonucleotides used in this work using standard phosphoramidite chemistry. DNA phosphoramidites and synthesis reagents were purchased from Glen Research (Sterling, VA, USA). Biosynthesis reagent grade acetonitrile was purchased from VWR (Mississauga, ON, Canada). Oligonucleotides were cleaved from the CPG beads (1,000 Å controlled pore glass) by incubation in ammonium hydroxide at 55°C, overnight, and then were purified by PAGE, desalted with Amicon Ultra Centrifugal Filter Units (3 K NMWL, 0.5 mL: Millipore, Billerica, MA, USA), and quantified by UV-Vis spectroscopy. Two DNA templates were used to prepare the selection library: (1) a novel pool (5′-ATAGTCCCATCATTC ATT-N30-AGATATTAGCAAGTGTCA-3′) and (2) a mutant pool based on the M5-15 aptamer, which had been previously selected to bind to αSyn.[30] The sequence of the M5-15 aptamer was 5′- atagtccc atcattcattGTATGGTACGGCGCGGTGGCGGGTGCGTGGagatatta gcaagtgtca-3′ where the primer domains are shown in lower case letters and the bases mutated by 30% are shown in capital letters. The primers used for PCR in the selection experiment were as follows: 5′-FAM-ATAGTCCCATCATTCATT (forward) and 5′-AAAAAAA AAAAAAAAAAAAA-HEG-TGACACTTGCTAATATCT (reverse).

Modified SELEX experiment for inhibitory aptamer selection

Selection conditions

The DNA selection library and αSyn (recombinant common human variant purchased from rPeptide, Bogart, GA, USA) were each prepared in selection buffer (PBS: 137 mM NaCl, 2.7 mM KCl, 8.1 mM Na_2HPO_4, 1.8 mM KH_2PO_4) and mixed 1:1 for the incubation step. αSyn only samples absent of any DNA were prepared in selection buffer to serve as aggregation controls. Stringency pressure was increased by varying the amount of DNA and protein each round[59] as well as by changing the buffer pH and the incubation times. See Table S3 for a summary of these parameters. In rounds 1–3, aggregation was induced by flash freezing in LN_2 and overnight lyophilization using a Labconco lyophilizer (Fisher Scientific, Ottawa, ON, Canada). The dried sample was then suspended in 180 μL DIH_2O water (18 MΩ cm) and placed on an incubator (180 RPM at 37°C). Selection rounds 4 and 5 were placed directly on the incubator without flash freezing. Table S3 summarizes the incubation time used for each round.

Ultracentrifugal fractionation

After incubation, unbound DNA and protein-DNA complexes were partitioned using ultracentrifugation. An OptiPrep density gradient (Sigma-Aldrich, St. Louis, MO, USA) was prepared by layering different percent solutions of OptiPrep in 5 mL thermal sealing ultracentrifuge tubes (Beckman, Brae, CA, USA). In selection round 1, layers of 35% (0.71 mL), 25% (2.14), and 2.5% (2.4 mL) comprised the gradient. Round 2 gradient was made up of 35% (1.0 mL), 25% (1.0 mL), 12% (1.0 mL), 6% (1.0 mL), 2.5% (1.0 mL), and 1% (0.6 mL). Rounds 3, 4, and 5 gradients consisted of layering 35% (1.0 mL), 25% (1.0 mL), 20% (1.0 mL), 12% (1.0 mL), 6% (1.0 mL), and 2.5% (0.6 mL). The products of the incubation were carefully loaded onto each density gradient and the tubes were sealed (Beckman Tube Sealer). See Table S4 for details on the centrifugation speeds for each round. After the samples were spun, 200-μL (rounds 1 and 2) or 250-μL (rounds 3–5) aliquots were taken from the top of the tube. Fractions were tested for the presence of fluorescein-labeled DNA using λex = 494 nm and λem = 520 nm (Fluorolog, Horiba Jobin Yvon Inc., Edison, NJ, USA) in order to pinpoint the fractions containing free DNA and DNA bound to different protein aggregates. Furthermore, the location of the bands of a protein ladder control (Precision Plus Protein All Blue Standard: Bio-Rad Laboratories, Hercules, CA, USA) added to the same gradient was analyzed by 5% non-denaturing PAGE to help assess the molecular mass corresponding to each fraction. The fluorescent DNA and protein were visualized in the non-denaturing polyacrylamide gel by excitation of the fluorescein at 302 nm and staining with Stains-All (Sigma-Aldrich), respectively.

The combination of these data helped to determine several fractions of interest; namely unbound DNA, and DNA-monomer complex, DNA-oligomer complex, and DNA-aggregate complex.

Secondary incubation

After fractionation but prior to TEM characterization, a secondary incubation period was used to apply extra stringency to the selection. In this way, any inhibition of aggregation exerted by the DNA library could be assessed by the difference in the TEM images. The length and temperature of the secondary incubation period was also varied by round: 130 h (at 4°C), 4 h (room temperature), 48 h (room temperature), for rounds 2, 3, and 4, respectively.

TEM or SEM assessment of aggregation

In order to visualize the protein morphology within each of the relevant fractions, electron microscopy was employed. Four microliters of each fraction were carefully deposited on Carbon-coated copper grids (CF300-Cu: Electron Microscopy Sciences, Hatfield, PA, USA) and left for 10 min, after which the excess sample was removed and the grids were left to dry at room temperature (RT). TEM images were obtained using an FEI Tecnai G2 F20 TEM (Hillsboro, OR, USA) equipped with a Gatan ORIUS TEM CCD Camera (Pleasanton, CA, USA) imaging system; beam voltage 120 kV. SEM images were obtained using a JEOL JSM-7500F Field Emission SEM, 30 kV.

DNA-protein complex partitioning by nitrocellulose filtration

Following the secondary incubation, the highest affinity sequences bound to monomer protein were isolated using nitrocellulose filtration. Nitrocellulose filters (0.45 μm HA: Millipore) were soaked in 1 mL of 0.5 M KOH for 20 min while shaking and then were washed four times with 100 mL each of deionized water. A 200-μL sample of the fractions of interest were passed over the pretreated membrane using a Swinnex filter mount (Millipore) attached to a 1-mL syringe. The retained DNA-protein complexes were eluted off the membrane using 1 mL of urea elution buffer (7 M urea, 0.05 M HEPES, pH 7.5) with agitation for 20 min then heating to 95°C for 15 min.

DNA recovery by phenol-chloroform extraction and ethanol precipitation

To denature the DNA-protein complexes, an equal volume of phenol:chloroform, isoamyl alcohol (25:24:1; BioShop Canada Inc., Burlington, ON, Canada) was added to the filter eluate. After brief agitation and centrifugation (12,000 × *g* for 5 min), the aqueous layer was removed, and extracted an additional two times with fresh equivolume aliquots of phenol:chloroform, isoamyl alcohol. A chloroform extraction was also performed to remove any residual phenol from the aqueous layer.

Ethanol precipitation was used to recover the DNA. Briefly, 100 μL of sodium acetate was added to the aqueous phase and was agitated by vortexing. Pre-chilled ethanol (2.75 mL) was added to the aqueous phase. After a brief agitation by vortexing, the solution was placed on ice for 20 min, and centrifuged (12,000 × *g*) for 15 min. The supernatant was removed and the pellet was resuspended in 500 μL of deionized water. The solution was desalted using Amicon Ultra Centrifugal Filter Units (3 K NMWL, 0.5 mL: Millipore, Billerica, MA, USA). The presence of DNA following these steps was confirmed using fluorescence spectroscopy.

PCR amplification of the enriched library

Following every selection round, 60 PCR reactions were prepared to amplify the enriched library. In addition, control reactions were also prepared, namely the negative (no template control) and the positive (template control). Reagents in the PCR mastermix were in the following proportions (for every 15 reactions): 750 μL of 2xFlumag Buffer (100 mM KCl, 200 mM Tris, 2% Triton X-100, pH of 9.0), 555 μL of deionized water, 120 μL of $MgCl_2$, 30 μL of dNTPs (BioShop Canada Inc.), 7.5 μL of each of the 0.2-mM primer solutions. TAQ DNA polymerase (15 μL; BioShop Canada, Inc.) was added to the mastermix and with gentle mixing by repeated pipetting. PCR reactions were prepared by aliquoting 99 μL of the mastermix into each tube, then adding 1 μL of pool, water, or template. The following thermal program was used on a thermal cycler (Eppendorf): 94°C (10 min), 30 × [94°C (1 min), 47°C (1 min), 72°C (1 min)], 72°C (10 min), 4°C (10 min). The PCR product was purified by denaturing PAGE (12%). The forward primer was labeled with fluorescein, which permitted the visualization of the amplified library by fluorescence excitation at 302 nm. The reverse primer was extended with a poly A20 tail, which allowed for a resolvable separation of the selection library forward strand and its complement by size. The library was eluted by crush and soak using deionized water ON, followed by desalting using Amicon Ultra Centrifugal Filter Units (3 K NMWL, 0.5 mL: Millipore, Billerica, MA, USA) and quantification by UV-Vis.

High-throughput sequencing and bioinformatic analysis of selection data

MiSeq sequencing

DNA from selected positive, negative, and counter pools were characterized using high-throughput sequencing. The pools were prepared for sequencing via amplification with specially designed forward and reverse primers containing barcode regions, which allowed for the analysis of multiple pools in one experiment. See Table S5 for the primer sequences used. The PCR mastermix and reactions were prepared as described for SELEX with the exception that the elongated primer pairs were used where appropriate. The amplification thermal profile was 94°C (10 min), 17 × [94°C (1 min), 58°C–60°C (1 min), 72°C (1 min)], 72°C (10 min), then finally 4°C (10 min). The PCR product was purified using 12% denaturing PAGE, desalted as previously described, and then quantified using a NanoDrop 1000 Spectrophotometer (Thermo Fisher, Waltham, MA, USA). The sequencing experiment was done on an Illumina MiSeq Instrument (Illumina, San Diego, CA, USA) as directed with the exception that the PhiX amount used was increased from the recommended value of ≥5%–20% to account for the low diversity of the libraries. The MiSeq Reagent Kit v2

(300 cycle) kit and PhiX CONTROL V3KIT required were purchased from Illumina.

Bioinformatic analysis of sequencing data using AptaCluster

Sequencing data were exported from the MiSeq Illumina System as FASTQ formatted files to Basespace.illumina.com. The AptaTools software suite was used to analyze the sequencing data[37,60] according to the AptaCLUSTER manual available online: https://www.ncbi.nlm.nih.gov/CBBresearch/Przytycka/index.cgi#aptaclustermanual. Raw sequence count, pool fraction, and selection cycle-to-cycle enrichment were extracted for each sequence. From these data, five aptamer hits were identified.

Inhibition of αSyn aggregation by aptamer hits

Aptamers were assessed for their ability to specifically inhibit fibril formation. Aptamers and αSyn monomer were each prepared in 1x Dulbecco's PBS (Sigma-Aldrich) to produce a final concentration of ∼5 mg/mL of each component. Aliquots (41 μL) of human αSyn monomer for PFFs (Proteos, Kalamazoo, MI, USA) at approximately 5 mg/mL (346 μM) were aliquoted into seven 1.5 mL amber microcentrifuge tubes, one for each of the five aptamer candidates, an M5-15 aptamer control, and an αSyn-only control. Into each reaction, a small volume (7–9 μL) of concentrated aptamer stock solution was added, yielding a final aptamer concentration of 346 μM, which was diluted to a final volume of 50 μL using 1x PBS. The incubation reactions were agitated briefly by vortexing then were placed on an incubator/shaker at 37°C and 300 RPM for 7 days. On each day, aliquots were removed for TEM imaging and Thioflavin T fluorescence assay. Thioflavin T (ThT) stock solution was prepared with 0.0128 g of ThT dissolved in 40 mL of 1x DPBS. The working ThT solution was produced fresh each day by diluting 25 μL of the stock solution with 975 μL of 1x DPBS. Each aptamer candidate was combined with αSyn PFFs in a 1-to-1 molar ratio and diluted with 1x DPBS to bring the volume of the working solutions to 50 μL. An αSyn control was also prepared to the same final concentration in 50 μL of 1x DPBS; 2.5μL of each sample was mixed with 95 μL of the working ThT solution and allowed to stand for 2 min. The solutions were then diluted 1:10 with 1x DPBS in triplicate. Sample fluorescence was tested by exciting the sample at 440 nm and detecting emission at 482 nm. The samples were incubated at 37 °C at 135 RPM for 7 days and the ThT protocol was followed for each sample again.

Assessment of aptamer binding affinity *in vitro*

Microscale thermophoresis

In vitro binding specificity of the aptamer hits for αSyn were initially assessed using microscale thermophoresis (MST). 5′-Cy5-tagged aptamers (5 μL of 100 μM) were dissolved in PBS (pH = 7.4) with 0.1% Tween 20, and dry αSyn monomer protein (rPeptide), A53T mutant αSyn (rPeptide), β-synuclein (rPeptide), or γ-synuclein (rPeptide) and characterized by MST (2Bind; Germany). Binding affinity was measured at a constant aptamer concentration (50 nM). Serial dilutions of αSyn protein were prepared at concentrations that ranged from 305 pM to ∼10.0 μM. Samples were analyzed using a Monolith NT.115 Pico at 25°C, which had 60% LED power and 40% laser power.

Electrochemical impedance spectroscopy

A CHI660C electrochemical workstation was used for all electrochemical measurements. A three-electrode electrochemical cell configuration was employed comprising an oligonucleotide-modified gold electrode (diameter 1.6 mm) working electrode, an Ag/AgCl 1 M KCl electrode reference electrode, and a platinum wire (diameter 2 mm) counter electrode. The 15 μL electrochemical cell was enclosed within a grounded Faraday cage. Thiol-modified oligonucleotides were suspended in 10 mM TCEP, 1 M NaCl, 10 mM phosphate, pH 7.4 for 60 min with constant agitation. Gold working electrodes were polished for 3 min in aqueous slurries containing 0.3 μm and 0.05 μm alumina and diamond powders, respectively (BASi, USA). Polished working electrodes were immersed in freshly prepared piranha solution (3:1 [v/v] 98% H_2SO_4/30% H_2O_2) for 3 min at 25°C. Electrodes were extensively rinsed with DiH_2O prior to electrochemical cleaning in 1 M H_2SO_4 where potential scanning between −0.25 V and 1.6 V until a reproducible cyclic voltammogram was produced. Freshly thiolated oligonucleotides were heated to 90°C for 5 min and cooled to 25°C prior to electrode immobilization. Gold electrode incubation in 1 μM oligonucleotide solution occurred for 2 h at 25°C followed by an extensive DiH_2O rinse and subsequent 60-min incubation in 1 mM MCH. The electrodes were washed in 10 mM NaCl, 5 mM Tris, pH 7.4 for 10 min with soft stirring before being dried under argon. EIS measurements were performed in PBS containing 5 mM $[Fe(CN)_6]^{3-/4-}$ and 0.1 M KCl with a frequency range of 0.01–100 kHz and a signal amplitude of 5 mV. The electrode was subjected to varying concentrations of monomeric αSyn for 60 min at 25°C and thoroughly rinsed with PBS to remove unbound target. Impedance changes were recorded before and after αSyn incubation in terms of charge transfer resistance (R_{ct}). EIS spectra were displayed as a Nyquist plot ($-Z_{im}$ vs. Z_{re}) using CHI software and fitted with a theoretical curve corresponding to Randles equivalent circuit. Each measurement was repeated four times, and control experiments for αSyn A53T mutant, αSyn fibril, β-synuclein, γ-synuclein, and thrombin control were carried out in identical conditions.

DNase I assay

Dilutions of αSyn (30 μM, 3 μM, 0.6 μM, 0.12 μM, 0.024 μM, and 0.0048μM) were prepared from a 5-mg/mL stock solution of αSyn monomer using 1x Dulbecco's PBS (Sigma-Aldrich). Aliquots of 20 μL of each αSyn dilution were combined with 20 μL of 10 μM 5′-fluorescein-labeled aptamer and the samples were incubated at 37°C for 1 h with mild agitation. In addition, two protein-free controls were prepared containing 20 μL of 10 μM aptamer and 20 μL of 1x PBS and incubated at 37°C for 1 h. Post incubation, the αSyn dilution series and one of the aptamer controls were treated with DNase I (Sigma-Aldrich) for 15 min at RT. An equivalent volume of formamide was added to each solution and then the solutions were loaded onto a multi-lane 19% denaturing PAGE with 1X TBE (0.089 M Tris, 0.089 M Boric Acid, 0.002 M EDTA) running buffer (300 V for 3.5 h). The gel was imaged using an AlphaImager and

analyzed using the SpotDenso feature of the AlphaImager software. Relative fluorescence of the respective bands in each lane were compared to generate a binding isotherm from which an apparent dissociation constant was approximated. The standard curve analysis (four parameter logistic curve) feature of SigmaPlot (Version 10.0: Systat Software, Inc.) was used to fit the relative fluorescence data based on the following equation:

$$y = +\left((max - min) \Big/ \left(1 + \left(\frac{x}{EC50}\right)^{Hillslope}\right)\right)$$

where y = relative fluorescence, x = αSyn concentration, min = minimum relative fluorescence value that can be obtained, max = maximum relative fluorescence value that can be obtained, EC50 is the point of inflection of the curve and the apparent K_D,[61] and Hillslope corresponds to the steepness of the curve at the inflection point.

The reported apparent dissociation constant represents the average of three bands and the error represents the standard deviation between the predicted values of the apparent K_Ds.

Cell culture

An SH-SY5Y human neuroblastoma cell line was donated by Dr. David Park. Cells were maintained in a complete media solution (Dulbecco's modified Eagle's medium [DMEM] containing 10% fetal bovine serum [FBS], 1% penicillin/streptomycin) at 37°C in a humified 95% air 5% CO_2 incubator. Once confluency (over 80%) was reached, cells were detached with a 1X TrypLE solution (ThermoFisher, cat#12605010) and plated at a density of 1×10^4 cells/well on a coated poly-D-Lysine (1:1,000) and Laminin (1:1,000) coverslip in a 24-well plate. Cell plate coating was allowed to incubate in wells with DMEM for 2 h before plating. Media changes were performed every 48 h for 7 days with a mixture of 0.1% retinoic acid and a complete cell media solution.

PFFs preparation

αSyn PFFs were prepared from recombinant human WT αSyn monomers (1-mg aliquot, Proteos). αSyn monomers were first thawed on ice for approximately 3 h and then underwent centrifugation at 4 °C at 14.8*g* for 10 min. The supernatant was obtained and placed in a sterile 1.5-mL microcentrifuge tube. The amount of supernatant obtained was used to determine the protein concentration of αSyn monomers using the A280 protein method from a NanoDrop 2000 Spectrophotometer (Thermo Fisher). The protein concentration of the supernatant was calculated using Beer's Law. The aliquot of αSyn monomers was then diluted with 10x DPBS to reach a final concentration of 5 mg/mL and vortexed for 3 s. Parafilm was wrapped around the lid to prevent evaporation and placed in an Eppendorf Thermomixer R (Fisher Scientific) at 37 °C at 1,000 RPM for 7 days. Once completed, the solution was aliquoted into 20 μL samples using gel loading pipet tips and allowed to freeze on dry ice before being stored at −80°C until experimental use.

Immunocytochemistry

Cells were fixed with 2% paraformaldehyde (PFA) in PBS for 15 min, then washed 3 × 5 min in PBS. Following the washes, the fixed cells were blocked and permeabilized with 2% bovine serum albumin (BSA) + 0.1% Triton X- in PBS for 30 min. Next, a primary antibody solution containing anti-αSyn filament antibody (1:1,000, Abcam, cat# ab209538) in 2% BSA in PBS was applied to cells for 1 h. Once the primary incubation elapsed, the cells were washed with PBS for 3 × 5 min. Afterward, cells were incubated with a secondary antibody solution containing anti-rabbit Alexa Fluro Plus 488 antibody (1:1,000, Fisher Scientific, cat# PIA32731) for 30 min at RT in 2% BSA in PBS. Following the antibody incubation, cells were stained with 4′,6-diamidino-2-phenylindole (DAPI) (1:10,000, Fisher Scientific, cat# PIEN62248). Finally, cells were washed 3 × 5 min before being imaged using the EVOS FL Imaging System (ThermoFisher, USA).

Quantification of αSyn aggregation deposits

Five sample areas were randomly taken within each well using the EVOS FL Imaging System (ThermoFisher, USA). A total of 10 cells were analyzed per experimental treatment and averaged for a single mean. All experimental data were performed in triplicates. αSyn aggregation was measured by the total intensity of cell area minus background and represented as mean integrated density.

Data analysis

All data are displayed as mean ± SEM. Data were analyzed using Levene's test and Shapiro-Wilk test to measure data normality and equal variances, respectively. The data were analyzed with one-way ANOVA or two-way ANOVA as indicated, and post hoc comparisons were performed using Tukey's HSD. Significant differences were set at $p < 0.05$.

αSyn PFF treatment

Cells were exposed to increasing concentrations of αSyn PFFs (0 μg/mL, 5 μg/mL, 10 μg/mL, and 25 μg/mL) for 3 days. αSyn PFFs were sonicated in pulses at approximately 1 pulse per second for 60 s before use. In experiment 2, cells were incubated with 5 μg/mL αSyn PFFs at 37°C and 5% CO_2 for either 1 h, 2 h, 4 h, or 8 h. Each experiment was performed in triplicate.

αSyn PFF and a-syn-1 treatments

Cells were exposed to αSyn PFFs (5 μg/mL) alone or combined with CY5-labeled a-syn-1 or non-labeled scrambled aptamer sequences. The sequence of the scrambled control was: 5′-GAT CAT GTA AGT GCG TGA GAG CGA GTA GCT CGA CAC GAA TCA GAA TAC ATT GCC GCT GTG TTA TAA-3′. αSyn PFFs were sonicated in pulses at approximately 1 pulse/second for 60 s before use. Stock concentrations of 5 μM and 10 μM aptamer sequences were added to the cells at 10% of the total well volume (500 μL), diluting to a final concentration of 0.5 μM and 1 μM. Following αSyn PFF and aptamer administration, cells were incubated at 37°C and 5% CO_2 for either 1 h, 2 h, 4 h, or 8 h. Experiments were performed in triplicate. Quantification and data analysis was done as described above.

In vivo analyses

Preparation of a-syn-1 aptamer loaded-TRAM liposomal delivery vehicle

A-syn-TRAM was produced as described previously.[25] Briefly, stock solutions of lipids for the production of liposomes were created by dissolving the following: 100 mg of POPC (16:0 18:1 PC Palmitoyloleoylphosphatidylcholine) was dissolved in 8 mL of chloroform, 1 mg of DDAB (Didodecyldimethylammonium bromide) was dissolved in 1 mL of chloroform, and 1 mg DSPE-PEG 2000 (1,2-distearoyl-sn-glycero-3-phosphoethanolamine-N-[amino(polyethylene glycol)-2000] (ammonium salt)) was dissolved in 1 mL of chloroform.

An aliquot of 1.17 mL (19.2 μmol) of the POPC stock solution, 126.3 μL (273 nmol) of the DDAB stock solution, and 88.25 μL (606 nmol) of the DSPE-PEG 2000 stock solution were transferred into a 10-mL round bottom flask containing 1.7 mg (30 nmol) DSPE-PEG 2000 maleimide (1,2-distearoyl-sn-glycero-3-phosphoethanolamine-N-[maleimide(polyethylene glycol)-2000] (ammonium salt)). The flask was capped with a septum and placed under a steady flow of argon along with gentle agitation to yield a thin, dry uniform lipid film. The lipid film was rehydrated with 0.2 mL of 50 mM TRIS-HCl, at pH 7.0, and vortexed for 30 min. The flask was stored under argon and sonicated in a bath sonicator at RT for 10 min; 38 nmol of 5′-Cyanine 3.5-labeled **a-syn-1** aptamer was added to the flask in a volume of 0.2 mL using 50 mM TRIS-HCl, at pH 7.0. To encapsulate the aptamer in the hydrated lipid film, 0.6 mL of 67% ethanol was slowly added to the flask; giving a final concentration of 40% ethanol in solution. The flask was stored under argon and underwent 10 freeze-thaw cycles (5 min in an ethanol/dry ice bath and 2 min in a 40°C water bath per cycle). Following the final freeze-thaw cycle, the liposome samples were extruded by undergoing 25 passes through a 100 nm polycarbonate membrane in a mini-extruder. The samples were dialyzed using 20,000 molecular weight Cut-Off Slide-A-Lyser cassettes (Thermo Scientific) into 50 mM HEPES buffer, at pH 7.0, overnight. To remove DNA that was non-specifically interacting with the liposome shell, nuclease digestion was performed using DNase I (Sigma-Aldrich) for 10 min. The samples were dialyzed into 50 mM HEPES buffer, at pH 7.0, overnight to remove the digested DNA from the samples. An aliquot of 120 nmol of thiol-modified transferrin receptor aptamer (TRA) was combined with 75 μL of 50 mM TRIS-HCl, at pH 8.4, containing 100 mM DL-dithiothreitol (DTT) and mixed by vortex at RT to cleave the disulfide bond on the TRA. Following the thiol cleavage, the TRA was purified using biospin columns (Bio-Rad Laboratories) then buffer exchanged into 50 mM HEPES buffer, at pH 7.0, containing 7 mM EDTA. The TRA solution was added to the liposome suspension and incubated at RT with gentle agitation. The samples underwent dialysis overnight into 50 mM HEPES buffer, at pH 7.0, to remove the EDTA and unreacted TRA.

The aptamer concentration was characterized using UV-Vis spectroscopy to maintain consistency between samples. To determine an approximate aptamer concentration, the Cyanine 3.5 peak, 590 nm, was observed with a 1:10 dilution of the liposome sample. The monodispersity of the liposomes was evaluated using TEM microscopy.

Preliminary assessment of A-syn-1 biodistribution

Subjects

Eighty male B6C3F1/J mice at 8–10 weeks of age were obtained from Jackson Laboratory, Bar Harbor, ME, and acclimated to the vivarium for 10 days prior to commencing the experiment. All mice were individually housed in standard polypropylene cages (27 × 21 × 14 cm) and maintained on a 12 h light/dark cycle with lights on at 08:00 h. A diet of 2014 Purina mouse chow and water was provided *ad libitum* and RT was maintained at ∼ 21°C. All procedures were approved by the Carleton University Animal Care Committee in accordance with the guidelines set out by the Canadian Council for Use and Care of Animals.

Experimental procedure

Mice were assigned to one of three treatment groups: (1) empty liposome (n = 16), (2) 100 μL **A-syn-TRAM** (n = 32), (3) 200uL **A-syn-TRAM** (n = 32). On the experimental test day, mice were administered an intraperitoneal (i.p.) injection with the assigned treatment. Mice within each treatment were further separated into one of four conditions determined by euthanasia time (15 min, 30 min, 1 h, 2 h; n = 4 empty liposome-treated mice per time point; n = 8, 100 μL **a-syn-1** aptamer treated mice per time point; n = 8, 200 μL **a-syn-1** aptamer treated mice per time point) following treatment. Thus, this experiment comprised a 3 (**a-syn-1** aptamer dose) × 4 (time between treatment and euthanasia) factorial design.

Brain extraction

Mice received an overdose of sodium pentobarbital (48 mg/kg i.p) and were transcardially perfused with 10 mL of phosphate buffered saline (0.01M PBS). Brain tissue (motor cortex and midbrain) and liver samples were collected for qPCR. Tissue was immediately frozen upon dissection and stored at −80°C until processing.

DNA isolation

Genomic DNA was isolated from each sample using a Qiagen DNEasy Blood & Tissue Kit (catalog # 69506) following kit instructions. Sample quality and concentrations were determined by absorbance at 280 nm and 260 nm with a NanoDrop Lite spectrophotometer. Samples were diluted with DEPC-treated water to a concentration of 10 ng/μL.

RT-qPCR

Samples were stored at −20°C prior to analyses. RT-qPCR was conducted on all gDNA samples to determine Cq values using primers designed to detect **a-syn-1** aptamer. Five microliters of each gDNA sample were loaded into separate wells in a 96-well PCR plate. Two microliters of 10 mM forward primers (5′-ATA GTC CCA TCA TTC ATT -3′), 2 μL of 10 mM reverse primers (5′- TGA CAC TTG CTA ATA TCT- 3′), 1 μL of DEPC-treated water, and 10 μL Sybr Green Supermix with fluorescein (Bio-Rad Laboratories Inc., Hercules, CA) were added to each well. Samples were run in

triplicate along with non-template controls. The plate was run on CFX Connect Real-Time PCR Detection System (Bio-Rad) for 30 s at 90°C, followed by 40 cycles of the following settings: 10 s at 90°C for denaturing and 40 s at 60°C for annealing. The plate was then run at 65°C for 5 s, then to 95°C for 5 s, and back to 65°C to generate a melt curve by increasing temperature from 65°C to 95°C for 5 s. All primers were tested for amplification efficiency using the standard curve method, yielding efficiencies over 95%.

Assessment of αSyn aggregation

Subjects

Breeding pairs comprising six female mice hemizygous for Tg(SNCA) 83Vle (Catalog# 004479) and six male WT controls (Catalog# 00101) were obtained at 8–12 weeks from Jackson Laboratory, Bar Harbor, ME. At 10 days following arrival, six female B6; C3-Tg(Prnp-SNCA*A53T)83Vle/J mice and the six male WT mice were paired for breeding purposes. Breeding was arranged as monogamous pairings, where one male and one female were paired for a 2-week period before the male mouse was removed.

Offspring were group-housed (max four per cage) with littermates of the same sex in standard polypropylene cages (27 × 21 × 14 cm) and maintained on a 12 h light/dark cycle with lights on at 08:00 h. A diet of 2014 Purina mouse chow and water was provided *ad libitum* and the RT was maintained at ∼ 21°C. Both WT and hemizygous offspring male mice were weaned at 21 days of age. All procedures were approved by the Carleton University Animal Care Committee and complied with the guidelines set out by the Canadian Council for Use and Care of Animals.

Procedure

At 5 months of age, male mice were assigned to one of five experimental groups: (1) control WT (n = 12), (2) control transgenic mice (n = 12), (3) transgenic mice that received multiple treatments of TRAM loaded with scrambled aptamer sequence (n = 6), (4) transgenic mice that received a single treatment with TRAM loaded with **a-syn-1** aptamer (n = 12), and (5) transgenic mice that received multiple treatments of TRAM with **a-syn-1** aptamer (n = 12). Mice in the control treatment groups received 1, 0.1-mL injection of 0.9% saline daily for 5 days. The three treatment groups likewise received a single 0.1-mL injection on each of the 5 days. All injections were administered between 9:00 h and 12:00 h. The scrambled aptamer treatment group received their injections once daily for each of the 5 days. The single treatment **a-syn-1** group received the **a-syn-1** injection on the first day followed by saline injections daily on each of the remaining 4 days. Mice in the multiple treatment group received the **a-syn-1** aptamer treatment once daily for each of the 5 consecutive days. All animals were killed by rapid decapitation 7 days following the last injection.

Brain extraction

Following decapitation, brains were extracted from each mouse from each treatment group and used for western blot. Brains were quickly excised and placed on a chilled micro-dissecting block that contained slots (0.5 mm apart) for single-edged razor blades. After the brain was sliced, micro-punches from coronal sections were taken from the frontal cortex, motor cortex, caudate, and substantia nigra. All region punches were immediately placed on dry ice and stored at −80°C until protein extraction.

Protein extraction

On the day of extraction, 10 mL of RIPA-like extraction buffer (Fisher, Catalog #P189900) was mixed with one tablet of protease inhibitor cocktail (Roche's Complete Mini EDTA-free cat#1836170). Extraction buffer was added to each sample (150 μL) and brain tissue was sonicated. Samples were kept at RT for 15 min and centrifuged for 10 min at 12,000 RPM (13,800 × g) at 4°C. The supernatant in each sample tube was removed and the remaining liquid was used to determine protein concentration.

Protein content was quantified using Pierce's BCA Protein Assay Kit (ThermoFisher, catalog# 23227) in a 96-well microplate. Kit instructions were followed and sample quantification was determined using a microplate reader (Molecular Devices, Spectra Max 190) at 540 nm. Samples were preserved in 5X Loading Buffer in a ratio of 4:1. Samples were prepared to concentrations of 10 μg/μL of protein per sample for all brain regions. They were vortexed and heated for 5 min in a heat block set to 105°C. After heating, samples were placed on ice for 5 min and stored at −20°C until processing.

Western blot

Total protein was first determined using a REVERT total protein solution as previously described.[24] Following determination of total protein levels and appropriate washes in tris-buffered saline (TBS; pH 7.5; 2 × 5 min each), membranes were blocked for 60 min in a TBS solution containing 0.5% fish gelatin (Sigma). Membranes were then placed in a 0.5% fish gelatin TBS solution containing a purified mouse anti-αSyn oligomer (1:2,000; Sigma Syn33, Catalog# ABN2265) antibody for a period of 90 min in 0.05% fish gelatin in TBS with 0.1% tween. Following incubation in the primary antibody, membranes were incubated in infrared conjugate secondary antibody (Rabbit 800, LI-COR) at a concentration of 1:20,000 in a 0.5% fish gelatin TBS solution containing 0.2% tween and 0.01% SDS. Following three washes in TBS-T, protein bands were read for 6 min on a Licor Odyssy system (ThermoFisher) at the appropriate wavelength.

Protein quantification

To normalize total protein, the intensity of each lane in the revert stain was determined using a densitometric analysis tool with Image Studio Lite 5.2 (LI-COR Bioscience, Lincoln, NE, USA). After identifying the revert lane with the highest amount of signal, a ratio was created for each lane against the highest signal. The calculation is as follows:

Lane 1 ratio: (Lane 1 Signal)/(Highest Lane Signal)

In vivo fluorescence co-localization experiment

Mice expressing the human A53T variant αSyn were injected with 100 μL of the **a-syn-1**-loaded **a-syn-TRAM** liposomes (i.p.). After 30 min, brain tissue was collected and prepared for immunohistochemistry. Intraperitoneal delivery of **a-syn-1** to the brain and binding of the **a-syn-1** aptamer to αSyn was probed by examining fluorescence apposition of the anti-αSyn (phospho S129) antibody and Cy3.5 labeled **a-syn-1** aptamer using fluorescence microscopy (Figure 4: Olympus BX61 microscope [Olympus Canada Inc, Richmond Hill, Canada]).

DATA AND CODE AVAILABILITY

Data available upon written request to the corresponding authors. Interested parties should contact M.C.D. for selection and aptamer characterization data, and M.R.H. for cellular assay data.

SUPPLEMENTAL INFORMATION

Supplemental information can be found online at https://doi.org/10.1016/j.omtn.2024.102251.

ACKNOWLEDGMENTS

The authors gratefully acknowledge the following individuals for their technical expertise and assistance with this research: Dr. Emily Mastronardi, Dr. Anna Koudrina, Dr. Jianquan Wang, Dr. William Willmore, and Dr. Alex Wong of Carleton University; Dr. Yun Liu of the University of Ottawa; and Dr. David Park from the University of Calgary. The research was supported by the Natural Sciences and Engineering Council of Canada (NSERC; 03817 for MCD and 04656 for MRH), the Canadian Institutes of Health Research (CIHR; PJT-2019-162084), and the Michael J. Fox Foundation for Parkinson's Research (9924 and 9924.01).

AUTHOR CONTRIBUTIONS

Conceptualization of the work was done by E.M.M., D.C., K.V., M.R.H., and M.C.D. Data curation, Formal Analysis, Investigation, Methodology, Validation, and Visualization were contributed to by all authors. Funding acquisition, project administration, and supervision was done by E.M.M., M.R.H., and M.C.D.. Writing of the original draft was done by E.M.M., D.C., K.V., J.P.C., V.H.H., S.B., M.R.H., and M.C.D. Review and editing were completed by E.M.M., D.C., M.R.H., and M.C.D.

DECLARATION OF INTERESTS

M.C.D. is a section editor of *Molecular Therapy - Nucleic Acids*. The authors have a patent related to this work: WO2019079887A1. It is entitled: Aptamers as a therapeutic tool to prevent protein aggregation in neurodegenerative disease.

REFERENCES

1. Rocca, W.A. (2018). The burden of Parkinson's disease: a worldwide perspective. Lancet Neurol. *17*, 928–929. https://doi.org/10.1016/S1474-4422(18)30355-7.
2. Moustafa, A.A., Chakravarthy, S., Phillips, J.R., Gupta, A., Keri, S., Polner, B., Frank, M.J., and Jahanshahi, M. (2016). Motor symptoms in Parkinson's disease: A unified framework. Neurosci. Biobehav. Rev. *68*, 727–740. https://doi.org/10.1016/j.neubiorev.2016.07.010.
3. Cha, Y., Park, T.-Y., Leblanc, P., and Kim, K.-S. (2023). Current Status and Future Perspectives on Stem Cell-Based Therapies for Parkinson's Disease. J. Mov. Disord. *16*, 22–41. https://doi.org/10.14802/jmd.22141.
4. Kumari, S., Taliyan, R., and Dubey, S.K. (2023). Comprehensive Review on Potential Signaling Pathways Involving the Transfer of α-Synuclein from the Gut to the Brain That Leads to Parkinson's Disease. ACS Chem. Neurosci. *14*, 590–602. https://doi.org/10.1021/acschemneuro.2c00730.
5. Lashuel, H.A., Overk, C.R., Oueslati, A., and Masliah, E. (2013). The many faces of α-synuclein: from structure and toxicity to therapeutic target. Nat. Rev. Neurosci. *14*, 38–48. https://doi.org/10.1038/nrn3406.
6. Goedert, M., Jakes, R., and Spillantini, M.G. (2017). The Synucleinopathies: Twenty Years On. J. Parkinsons Dis. *7*, S51–S69. https://doi.org/10.3233/JPD-179005.
7. Sun, X., Dyson, H.J., and Wright, P.E. (2023). Role of conformational dynamics in pathogenic protein aggregation. Curr. Opin. Chem. Biol. *73*, 102280. https://doi.org/10.1016/j.cbpa.2023.102280.
8. Miraglia, F., Ricci, A., Rota, L., and Colla, E. (2018). Subcellular localization of alpha-synuclein aggregates and their interaction with membranes. Neural Regen. Res. *13*, 1136–1144. https://doi.org/10.4103/1673-5374.235013.
9. Sharma, M., and Burré, J. (2023). α-Synuclein in synaptic function and dysfunction. Trends Neurosci. *46*, 153–166. https://doi.org/10.1016/j.tins.2022.11.007.
10. Surguchov, A., and Surguchev, A. (2022). Synucleins: New Data on Misfolding, Aggregation and Role in Diseases. Biomedicines *10*, 3241. https://doi.org/10.3390/biomedicines10123241.
11. Meade, R.M., Fairlie, D.P., and Mason, J.M. (2019). Alpha-synuclein structure and Parkinson's disease – lessons and emerging principles. Mol. Neurodegener. *14*, 29. https://doi.org/10.1186/s13024-019-0329-1.
12. Giráldez-Pérez, R., Antolín-Vallespín, M., Muñoz, M., and Sánchez-Capelo, A. (2014). Models of α-synuclein aggregation in Parkinson's disease. Acta Neuropathol. Commun. *2*, 176. https://doi.org/10.1186/s40478-014-0176-9.
13. Jagmag, S.A., Tripathi, N., Shukla, S.D., Maiti, S., and Khurana, S. (2015). Evaluation of Models of Parkinson's Disease. Front. Neurosci. *9*, 503. https://doi.org/10.3389/fnins.2015.00503.
14. Visanji, N.P., Brotchie, J.M., Kalia, L.V., Koprich, J.B., Tandon, A., Watts, J.C., and Lang, A.E. (2016). α-Synuclein-Based Animal Models of Parkinson's Disease: Challenges and Opportunities in a New Era. Trends Neurosci. *39*, 750–762. https://doi.org/10.1016/j.tins.2016.09.003.
15. Polinski, N.K., Volpicelli-Daley, L.A., Sortwell, C.E., Luk, K.C., Cremades, N., Gottler, L.M., Froula, J., Duffy, M.F., Lee, V.M.Y., Martinez, T.N., and Dave, K.D. (2018). Best Practices for Generating and Using Alpha-Synuclein Pre-Formed Fibrils to Model Parkinson's Disease in Rodents. J. Parkinsons Dis. *8*, 303–322. https://doi.org/10.3233/JPD-171248.
16. Duffy, M.F., Collier, T.J., Patterson, J.R., Kemp, C.J., Fischer, D.L., Stoll, A.C., and Sortwell, C.E. (2018). Quality Over Quantity: Advantages of Using Alpha-Synuclein Preformed Fibril Triggered Synucleinopathy to Model Idiopathic Parkinson's Disease. Front. Neurosci. *12*, 621. https://doi.org/10.3389/fnins.2018.00621.
17. Giasson, B.I., Duda, J.E., Quinn, S.M., Zhang, B., Trojanowski, J.Q., and Lee, V.M.Y. (2002). Neuronal alpha-synucleinopathy with severe movement disorder in mice expressing A53T human alpha-synuclein. Neuron *34*, 521–533. https://doi.org/10.1016/S0896-6273(02)00682-7.
18. Ventura, K. (2021). The Use of a Novel Alpha-Synuclein Binding Aptamer in Models of Parkinson's Disease. https://doi.org/10.22215/etd/2021-14868.
19. Tuerk, C., and Gold, L. (1990). Systematic evolution of ligands by exponential enrichment: RNA ligands to bacteriophage T4 DNA polymerase. Science *249*, 505–510. https://doi.org/10.1126/science.2200121.
20. Ellington, A.D., and Szostak, J.W. (1992). Selection in vitro of single-stranded DNA molecules that fold into specific ligand-binding structures. Nature *355*, 850–852. https://doi.org/10.1038/355850a0.
21. McKeague, M., McConnell, E.M., Cruz-Toledo, J., Bernard, E.D., Pach, A., Mastronardi, E., Zhang, X., Beking, M., Francis, T., Giamberardino, A., et al. (2015). Analysis of In Vitro Aptamer Selection Parameters. J. Mol. Evol. *81*, 150–161. https://doi.org/10.1007/s00239-015-9708-6.

22. Ruigrok, V.J.B., Levisson, M., Eppink, M.H.M., Smidt, H., and van der Oost, J. (2011). Alternative affinity tools: more attractive than antibodies? Biochem. J. *436*, 1–13. https://doi.org/10.1042/BJ20101860.

23. Tolle, F., and Mayer, G. (2013). Dressed for success – applying chemistry to modulate aptamer functionality. Chem. Sci. *4*, 60–67. https://doi.org/10.1039/c2sc21510a.

24. Rusconi, C.P., Scardino, E., Layzer, J., Pitoc, G. a, Ortel, T.L., Monroe, D., and Sullenger, B. a (2002). RNA aptamers as reversible antagonists of coagulation factor IXa. Nature *419*, 90–94. https://doi.org/10.1038/nature00963.

25. McConnell, E.M., Ventura, K., Dwyer, Z., Hunt, V., Koudrina, A., Holahan, M.R., and Derosa, M.C. (2019). In Vivo Use of a Multi-DNA Aptamer-Based Payload/Targeting System to Study Dopamine Dysregulation in the Central Nervous System. ACS Chem. Neurosci. *10*, 371–383. https://doi.org/10.1021/acschemneuro.8b00292.

26. Ren, X., Zhao, Y., Xue, F., Zheng, Y., Huang, H., Wang, W., Chang, Y., Yang, H., and Zhang, J. (2019). Exosomal DNA Aptamer Targeting α-Synuclein Aggregates Reduced Neuropathological Deficits in a Mouse Parkinson's Disease Model. Mol. Ther. Nucleic Acids *17*, 726–740. https://doi.org/10.1016/j.omtn.2019.07.008.

27. Takahashi, T., Tada, K., and Mihara, H. (2009). RNA aptamers selected against amyloid beta-peptide (Abeta) inhibit the aggregation of Abeta. Mol. Biosyst. *5*, 986–991. https://doi.org/10.1039/b903391b.

28. Chaudhary, R.K., Patel, K.A., Patel, M.K., Joshi, R.H., and Roy, I. (2015). Inhibition of Aggregation of Mutant Huntingtin by Nucleic Acid Aptamers In Vitro and in a Yeast Model of Huntington's Disease. Mol. Ther. *23*, 1912–1926. https://doi.org/10.1038/mt.2015.157.

29. Rhie, A., Kirby, L., Sayer, N., Wellesley, R., Disterer, P., Sylvester, I., Gill, A., Hope, J., James, W., and Tahiri-Alaoui, A. (2003). Characterization of 2'-fluoro-RNA aptamers that bind preferentially to disease-associated conformations of prion protein and inhibit conversion. J. Biol. Chem. *278*, 39697–39705. https://doi.org/10.1074/jbc.M305297200.

30. Tsukakoshi, K., Harada, R., Sode, K., and Ikebukuro, K. (2010). Screening of DNA aptamer which binds to alpha-synuclein. Biotechnol. Lett. *32*, 643–648. https://doi.org/10.1007/s10529-010-0200-5.

31. Tsukakoshi, K., Abe, K., Sode, K., and Ikebukuro, K. (2012). Selection of DNA aptamers that recognize α-synuclein oligomers using a competitive screening method. Anal. Chem. *84*, 5542–5547. https://doi.org/10.1021/ac300330g.

32. Tran, C.H., Saha, R., Blanco, C., Bagchi, D., and Chen, I.A. (2022). Modulation of α-Synuclein Aggregation In Vitro by a DNA Aptamer. Biochemistry *61*, 1757–1765. https://doi.org/10.1021/acs.biochem.2c00207.

33. Zheng, Y., Qu, J., Xue, F., Zheng, Y., Yang, B., Chang, Y., Yang, H., and Zhang, J. (2018). Novel DNA Aptamers for Parkinson's Disease Treatment Inhibit α-Synuclein Aggregation and Facilitate its Degradation. Mol. Ther. Nucleic Acids *11*, 228–242. https://doi.org/10.1016/j.omtn.2018.02.011.

34. Hmila, I., Sudhakaran, I.P., Ghanem, S.S., Vaikath, N.N., Poggiolini, I., Abdesselem, H., and El-Agnaf, O.M.A. (2022). Inhibition of α-Synuclein Seeding-Dependent Aggregation by ssDNA Aptamers Specific to C-Terminally Truncated α-Synuclein Fibrils. ACS Chem. Neurosci. *13*, 3330–3341. https://doi.org/10.1021/acschemneuro.2c00362.

35. Xiao, X., Li, H., Zhao, L., Zhang, Y., and Liu, Z. (2021). Oligonucleotide aptamers: Recent advances in their screening, molecular conformation and therapeutic applications. Biomed. Pharmacother. *143*, 112232. https://doi.org/10.1016/j.biopha.2021.112232.

36. DeRosa, M.C., Lin, A., Mallikaratchy, P., McConnell, E.M., McKeague, M., Patel, R., and Shigdar, S. (2023). In vitro selection of aptamers and their applications. Nat. Rev. Methods Primers *3*, 54. https://doi.org/10.1038/s43586-023-00238-7.

37. Hoinka, J., Berezhnoy, A., Sauna, Z.E., Gilboa, E., and Przytycka, T.M. (2014). AptaCluster - A Method to Cluster HT-SELEX Aptamer Pools and Lessons from its Application. Res. Comput. Mol. Biol. *8394*, 115–128. https://doi.org/10.1007/978-3-319-05269-4_9.

38. Mathews, D.H. (2014). RNA Secondary Structure Analysis Using RNAstructure. Curr. Protoc. Bioinformatics *46*, 12.6.1–12.6.25. https://doi.org/10.1002/0471250953.bi1206s46.

39. Luo, X., McKeague, M., Pitre, S., Dumontier, M., Green, J., Golshani, A., Derosa, M.C., and Dehne, F. (2010). Computational approaches toward the design of pools for the in vitro selection of complex aptamers. RNA *16*, 2252–2262. https://doi.org/10.1261/rna.2102210.

40. Volpicelli-Daley, L.A., Luk, K.C., and Lee, V.M.-Y. (2014). Addition of exogenous α-synuclein preformed fibrils to primary neuronal cultures to seed recruitment of endogenous α-synuclein to Lewy body and Lewy neurite–like aggregates. Nat. Protoc. *9*, 2135–2146. https://doi.org/10.1038/nprot.2014.143.

41. The Michael, J.. Fox Foundation for Parkinson's Research Protocol for Generation of Pre-formed Fibrils from Alpha-Synuclein Monomer. Preprint. https://www.michaeljfox.org/sites/default/files/media/document/PFF%20Protocol%202017b.pdf.

42. Frost, N.R., McKeague, M., Falcioni, D., and DeRosa, M.C. (2015). An in solution assay for interrogation of affinity and rational minimer design for small molecule-binding aptamers. Analyst *140*, 6643–6651. https://doi.org/10.1039/C5AN01075F.

43. McKeague, M., De Girolamo, A., Valenzano, S., Pascale, M., Ruscito, A., Velu, R., Frost, N.R., Hill, K., Smith, M., McConnell, E.M., and DeRosa, M.C. (2015). Comprehensive Analytical Comparison of Strategies Used for Small Molecule Aptamer Evaluation. Anal. Chem. *87*, 8608–8612. https://doi.org/10.1021/acs.analchem.5b02102.

44. Breitsprecher, D., Schlinck, N., Witte, D., Duhr, S., Baaske, P., and Schubert, T. (2016). Aptamer Binding Studies Using MicroScale Thermophoresis. Methods Mol. Biol. *1380*, 99–111. https://doi.org/10.1007/978-1-4939-3197-2_8.

45. Montanari, J.A.M., Bucci, P.L., and Alonso, S.d.V. (2014). A model based in the radius of vesicles to predict the number of unilamellar liposomes. Int. J. Res. Pharm. Chem. *4*, 484–489.

46. Fujiwara, H., Hasegawa, M., Dohmae, N., Kawashima, A., Masliah, E., Goldberg, M.S., Shen, J., Takio, K., and Iwatsubo, T. (2002). alpha-Synuclein is phosphorylated in synucleinopathy lesions. Nat. Cell Biol. *4*, 160–164. https://doi.org/10.1038/ncb748.

47. Sengupta, U., Guerrero-Muñoz, M.J., Castillo-Carranza, D.L., Lasagna-Reeves, C.A., Gerson, J.E., Paulucci-Holthauzen, A.A., Krishnamurthy, S., Farhed, M., Jackson, G.R., and Kayed, R. (2015). Pathological Interface Between Oligomeric Alpha-Synuclein and Tau in Synucleinopathies. Biol. Psychiatr. *78*, 672–683. https://doi.org/10.1016/j.biopsych.2014.12.019.

48. Freitas, M.E., Hess, C.W., and Fox, S.H. (2017). Motor Complications of Dopaminergic Medications in Parkinson's Disease. Semin. Neurol. *37*, 147–157. https://doi.org/10.1055/s-0037-1602423.

49. Obeso, J.A., Olanow, C.W., and Nutt, J.G. (2000). Levodopa motor complications in Parkinson's disease. Trends Neurosci. *23*, S2–S7. https://doi.org/10.1016/S1471-1931(00)00031-8.

50. Parkinson Study Group CALM Cohort Investigators (2009). Long-term Effect of Initiating Pramipexole vs Levodopa in Early Parkinson Disease. Arch. Neurol. *66*, 563–570. https://doi.org/10.1001/archneurol.2009.32.

51. Bressman, S., and Saunders-Pullman, R. (2019). When to Start Levodopa Therapy for Parkinson's Disease. N. Engl. J. Med. *380*, 389–390. https://doi.org/10.1056/NEJMe1814611.

52. PD Med Collaborative Group, Gray, R., Ives, N., Rick, C., Patel, S., Gray, A., Jenkinson, C., McIntosh, E., Wheatley, K., Williams, A., and Clarke, C.E. (2014). Long-term effectiveness of dopamine agonists and monoamine oxidase B inhibitors compared with levodopa as initial treatment for Parkinson's disease (PD MED): a large, open-label, pragmatic randomised trial. Lancet *384*, 1196–1205. https://doi.org/10.1016/S0140-6736(14)60683-8.

53. Olanow, C.W., Watts, R.L., and Koller, W.C. (2001). An algorithm (decision tree) for the management of Parkinson's disease (2001): treatment guidelines. Neurology *56*, S1–S88. https://doi.org/10.1212/WNL.56.suppl_5.S1.

54. Massey, R.S., McConnell, E.M., Chan, D., Holahan, M.R., DeRosa, M.C., and Prakash, R. (2023). Non-invasive Monitoring of α-Synuclein in Saliva for Parkinson's Disease Using Organic Electrolyte-Gated FET Aptasensor. ACS Sens. *8*, 3116–3126. https://doi.org/10.1021/acssensors.3c00757.

55. Huang, Z., and Szostak, J.W. (2003). Evolution of aptamers with a new specificity and new secondary structures from an ATP aptamer. RNA *9*, 1456–1463. https://doi.org/10.1261/rna.5990203.

56. Wang, W., Perovic, I., Chittuluru, J., Kaganovich, A., Nguyen, L.T.T., Liao, J., Auclair, J.R., Johnson, D., Landeru, A., Simorellis, A.K., et al. (2011). A soluble α-synuclein construct forms a dynamic tetramer. Proc. Natl. Acad. Sci. USA *108*, 17797–17802. https://doi.org/10.1073/pnas.1113260108.

57. De Girolamo, A., McKeague, M., Pascale, M., Cortese, M., and DeRosa, M.C. (2018). Immobilization of Aptamers on Substrates. In Aptamers for Analytical Applications (Wiley)), pp. 85–126. https://doi.org/10.1002/9783527806799.ch3.

58. Lee, M.K., Stirling, W., Xu, Y., Xu, X., Qui, D., Mandir, A.S., Dawson, T.M., Copeland, N.G., Jenkins, N.A., and Price, D.L. (2002). Human α-synuclein-harboring familial Parkinson's disease-linked Ala-53 → Thr mutation causes neurodegenerative disease with α-synuclein aggregation in transgenic mice. Proc. Natl. Acad. Sci. USA *99*, 8968–8973. https://doi.org/10.1073/pnas.132197599.

59. Grey, M., Dunning, C.J., Gaspar, R., Grey, C., Brundin, P., Sparr, E., and Linse, S. (2015). Acceleration of α-synuclein aggregation by exosomes. J. Biol. Chem. *290*, 2969–2982. https://doi.org/10.1074/jbc.M114.585703.

60. Hoinka, J., Berezhnoy, A., Dao, P., Sauna, Z.E., Gilboa, E., and Przytycka, T.M. (2015). Large scale analysis of the mutational landscape in HT-SELEX improves aptamer discovery. Nucleic Acids Res. *43*, 5699–5707. https://doi.org/10.1093/nar/gkv308.

61. Müller, J., Freitag, D., Mayer, G., and Pötzsch, B. (2008). Anticoagulant characteristics of HD1-22, a bivalent aptamer that specifically inhibits thrombin and prothrombinase. J. Thromb. Haemostasis *6*, 2105–2112. https://doi.org/10.1111/j.1538-7836.2008.03162.x.